



Identification and implications of off-axis lava flows around the East Pacific Rise

Jennifer R. Reynolds

Lamont-Doherty Earth Observatory, Palisades, New York 10964
Now at Division of Earth and Ocean Sciences, Duke University, P. O. Box 90227, Durham,
North Carolina 27708 (jrr@eos.duke.edu)

Charles H. Langmuir

Lamont-Doherty Earth Observatory, Palisades, New York 10964 (langmuir@ldeo.columbia.edu)

[1] **Abstract:** Off-axis eruptions at ocean ridges provide critical information with respect to underlying crustal plumbing and mantle melting systems. A detailed study of basaltic glass samples around the East Pacific Rise from 12°00' to 12°30'N provides geological evidence for the existence of off-axis eruptions with a distinctive chemical composition. This composition has not been found along the axis of the EPR from 8° to 14°N except at a ridge-transform intersection but has been recovered in numerous locations that were farther than 1 km off axis. These off-axis normal mid-ocean ridge basalts, or OA-NMORB, are distinguished by low Na₂O, Sr, and Al₂O₃ and are unusually depleted in incompatible elements. Moderately enriched off-axis transitional mid-ocean ridge basalts (OA-TMORB) with the same compositional tendencies can also be identified. Comparison of EPR axis lavas and the OA type suggests that they come from the same range of (unmelted) mantle source compositions but that the source of the OA magmas was depleted in incompatible trace elements by removal of a small-degree partial melt. This would be consistent with the OA type as an EPR pooled melt that is missing the low-degree melt fraction from deep in the melting regime, which provides a reasonable physical model for their formation. In this case, off-axis magmas do not represent the same range of chemical variation as magmas delivered to the axial magma system. The OA-NMORB are similar to depleted lavas from near-EPR seamounts. Other seamount lavas with depleted trace elements have TMORB-like major elements, and may be classified as OA-TMORB. The similarity between seamount lavas and the lavas erupted off axis close to the EPR suggests that the two are manifestations of the same phenomenon. We suggest that seamount-type volcanism effectively starts within 1–2 km of the axis. This is within the range where lavas derived from the axial plumbing system may also erupt. Therefore there is a narrow zone where young lava flows from the axial plumbing system and from the off-axis systems may overlap. Lavas erupted off axis may ultimately cover 20% of the seafloor around the EPR, which is substantially more than previous estimates that were based primarily on morphological studies.

Keywords: East Pacific Rise; MORB; seamount; mantle melting; melt focusing; off axis.

Index terms: Mid-ocean ridge processes; igneous petrology; Pacific Ocean.

Received November 16, 1999; **Accepted** March 29, 2000;

Published June 13, 2000.



Reynolds, J. R., and C. H. Langmuir, 2000. Identification and implications of off-axis lava flows around the East Pacific Rise, *Geochem. Geophys. Geosyst.*, vol. 1, Paper number 1999GC000033 [13,181 words, 8 figures, 3 tables]. June 13, 2000.

1. Introduction

[2] The classical model of seafloor spreading has all lavas erupted at the spreading center axis, with the age of the volcanic surface increasing linearly with distance. Studies of the East Pacific Rise have shown a contrast between some lavas sampled on axis, at the center of the axial high, and those sampled off axis, on the flanks of the axial high and the adjacent abyssal hills. For example, *Reynolds et al.* [1992] showed a zonation of lavas in the 12°N region, not associated with seamounts, and suggested that the zonation reflected temporal changes in the lava delivered to the axis. Multiple studies have shown, however, that lavas at fast-spreading ridges are not erupted exclusively at the axis but also from near-ridge seamounts [e.g., *Batiza and Vanko*, 1984] and other off-axis sites [e.g., *Perfit et al.*, 1994a, b]. *Niu and Batiza* [1997, 1998] documented very large chemical variations of off-axis seamount lavas and suggested that they reflected more accurately the spectrum of magma compositions delivered from the mantle. The implicit assumption of these and other studies is that while on- and off-axis lavas may differ, the ranges of parental magmas for on-axis and off-axis volcanism are equivalent. The plumbing system on axis mixes and modifies the spectrum of parental magmas in diverse ways.

[3] An alternative view is that the mantle melting regime delivers different magmas on and off axis. Lavas erupted contemporaneously at different distances from the axis may sample a cross section of the magmas delivered from the mantle. This is implicit in earlier work by *Batiza et al.* [1989, 1990], for example. In this

scenario, because melts are produced by adiabatic decompression of the upwelling mantle, they would provide information about the spatial distribution of melt compositions that is relevant to the dynamics of mantle flow [e.g., *Wilson*, 1992; *Niu et al.*, 1996].

[4] These different perspectives raise the possibility that fast-spreading ridges provide the opportunity to investigate both spatial and temporal change in all levels of the magmatic system. To investigate these two discrete problems, however, it is necessary to be able to clearly distinguish lavas that are erupted on axis and carried off axis by spreading from lavas that are emplaced off axis. Resolution of these magma types then would discriminate between spatial and temporal changes in magma composition, with implications for both crustal and mantle processes.

[5] In theory, and on land, this resolution could be accomplished by detailed geological mapping and dating. Both of these are difficult to accomplish in the deep sea environment, and hence forward progress requires the development of additional approaches.

[6] In this paper, we report on samples from an intensive along- and across-strike investigation of the East Pacific Rise between 12°00' and 12°30'N. Dredging and rock coring in an area 50 km along axis and 18 km wide recovered 144 distinct compositions from 126 sampling locations [*Reynolds et al.*, 1992]. As documented below, these data show that many lava flows erupted off axis have a chemical composition that is distinguishable from lavas emplaced at the axis. The recognition of an exclusively off axis chemical type provides a



new tool to address several specific problems central to our understanding of fast-spreading ridges. (1) What is the width of the neovolcanic zone? (2) How common are off-axis eruptions, and to what extent do they interfere with investigations of temporal change by off-axis sampling? (3) Once the off-axis lavas are removed from consideration, what are the characteristics, scale, and magnitude of temporal change in East Pacific Rise magmatism? (4) What produces the off-axis lava type, and what implications does this have for melt generation and delivery beneath the East Pacific Rise?

2. Off-Axis Volcanism: Previous Evidence

[7] There is geological and geophysical evidence for lava flows outside the $\sim 300\text{--}600$ m wide axial summit trough of the northern East Pacific Rise (EPR). Seismic experiments in the 9°N region have shown that the seismic layer 2A, commonly regarded as the extrusive volcanic section, thickens by 200–300% between the axis and 1–1.5 km off axis [Harding *et al.*, 1993; Christeson *et al.*, 1996]. The seismic experiment closest to our sample locations, at $12^\circ 20'\text{--}13^\circ 00'\text{N}$, shows a 200–300% increase of layer 2A thickness over 1–2 km [Babcock *et al.*, 1998]. Even at the volcanically “starved” ridge north of 13° , the layer 2A thickness increases by $\sim 50\%$ over the same distance [Kappus *et al.*, 1995]. Some of the thickening of layer 2A might be attributed to shallow intrusions, i.e., sill formation within the volcanic pile, but most of it probably represents lava flows [e.g., Christeson *et al.*, 1996]. Estimates for the width of the zone of lava flows around the axis based on characteristics of the magnetic polarity transition are 0.6–2.0 km at the intermediate-spreading EPR at 21°N [Macdonald *et al.*, 1983] and 4–10 km at the superfast-spreading southern EPR at $19^\circ 30'\text{N}$ [Sempere *et al.*, 1987].

[8] How lavas may actually thicken layer 2A is not as clear. Some of the thickening appears to result from lavas erupted on axis that flow off axis. Studies of seafloor geology in the 9°N , 12°N , and 13°N regions show widespread evidence of lava flows that erupted in the neovolcanic zone and traveled 1–2 km from the axis. This is largely based on discrete steps in the thickness of sediment cover (but see *Perfit and Chadwick* [1998] for an alternative view). This interpretation has been supported by the results from recent *Alvin* dives on abyssal hills in the 9°N region [Macdonald *et al.*, 1996] and by stochastic modeling of dike injection and lava flow patterns [Hoofst *et al.*, 1996]. It has led to a general model in which the size and extent of lava flows on the northern EPR vary in cycles: At their maximum the flows travel down the slopes of the axial rise, generally as far as the first inward facing fault scarp [Gente *et al.*, 1986; Barone and Ryan, 1990; Reynolds, 1995].

[9] There is also evidence for eruptions through actual off-axis vents. From *Alvin* dives at $9^\circ 30'\text{N}$, *Perfit and Chadwick* [1998] and *Fornari et al.* [1998] describe steep-sided pillow ridges 5–20 m high, located along fissures and constructed of fresher-looking lava than the surrounding seafloor. This volcanic landform has not been observed anywhere along the EPR axis itself and probably represents small-volume eruptions through off-axis faults and fissures.

[10] Petrologic and geochemical studies are also relevant. The apparently asymmetrical distribution of enriched mid-ocean ridge basalt (EMORB) and transitional mid-ocean ridge basalt (TMORB) around the EPR axis in both the 12°N and 9°N regions has been tentatively attributed to off-axis eruption of enriched lavas [Reynolds *et al.*, 1992; Perfit *et al.*, 1994a]. Anomalously young ages of some off-axis basalts from 9°N that have been dated by U-



series isotopic disequilibrium constitute one of the strongest pieces of evidence for off-axis eruptions [Goldstein *et al.*, 1994].

[11] Other off-axis volcanism not apparently related to layer 2A thickening, i.e., seamount formation, has been known since the earliest studies of the EPR. Because subcircular volcanic cones are not found anywhere on the EPR axis itself, all such features are considered to form at off-axis vents. The larger near-ridge seamounts reach a height of >200 m at a distance of 5–15 km off the EPR axis and can continue to grow at least out to 30 km [Scheirer and Macdonald, 1995; Alexander and Macdonald, 1996]. The area of seafloor covered by such seamounts is estimated to be 6% [Scheirer and Macdonald, 1995]. Smaller volcanic edifices, subcircular features 40–200 m high, can also be unambiguously identified on SeaBeam maps that have 10 m resolution [Alexander and Macdonald, 1996]. Around the 9°N region these edifices cover 7–11% of the seafloor beyond 5 km off axis.

[12] Identifying off-axis volcanic constructions and lava flows becomes more difficult as their size decreases toward the resolution of the mapping systems and the relief of the abyssal hill terrain. Thus the line of demarcation (or zone of overlap) between active ridge axis volcanism and off-axis seamount volcanism has not been well defined. Side-scan sonar images, seafloor photographs, and submersible diving are useful in this regard, but they are only available for limited areas. The one existing geochemical method for identifying off-axis eruptions is dating by U-series isotopes [e.g., Goldstein *et al.*, 1994; Perfit and Chadwick, 1998], but this too is of limited use because it can only be done on a small number of samples and requires some assumptions about lava chemical composition and petrogenesis.

[13] Identification of individual off-axis flows not associated with seamounts is critical for an evaluation of spatial and temporal variations and yet is both difficult and expensive by geological methods alone. Other approaches would be valuable. Using samples for which the geological constraints are adequate, we have identified a chemical composition that is characteristic of off-axis volcanism and does not occur on axis. The chemical criteria can be used to distinguish an important class of off-axis flows, those that were actually erupted off axis independent of the axial magma reservoir. The ones that we identify are ≥ 1 km from the axial summit depression. They are compositionally distinct from those that were erupted on axis (or near axis, i.e., <2 km) from the axial magma system and carried off axis by seafloor spreading. The result provides a broader data set with which to investigate the scientific questions discussed above.

3. East Pacific Rise From 12°00' to 12°30'N

[14] Our study of basalts from the 12°00'–12°30'N region of the EPR recovered 61 samples between 0 and 1.0 km off axis and another 31 samples between 1 and 10 km off axis (Figure 1). All are from the 1989 Venture leg 2 cruise of the R/V *Thomas Washington*, in October 1989. The sampling precision during this cruise, the first to use rock coring [Reynolds *et al.*, 1992], was exceptional in comparison to classical dredging studies of ocean ridges. The development of the rock core technique, and real-time SeaBeam bathymetry matched to a Global Positioning System (GPS)-navigated base map [Monti *et al.*, 1987], enabled the recovery of rock core samples from the seafloor with locations known to 100 m. Of the 23 dredges during our survey, 9 were navigated by relay trans-

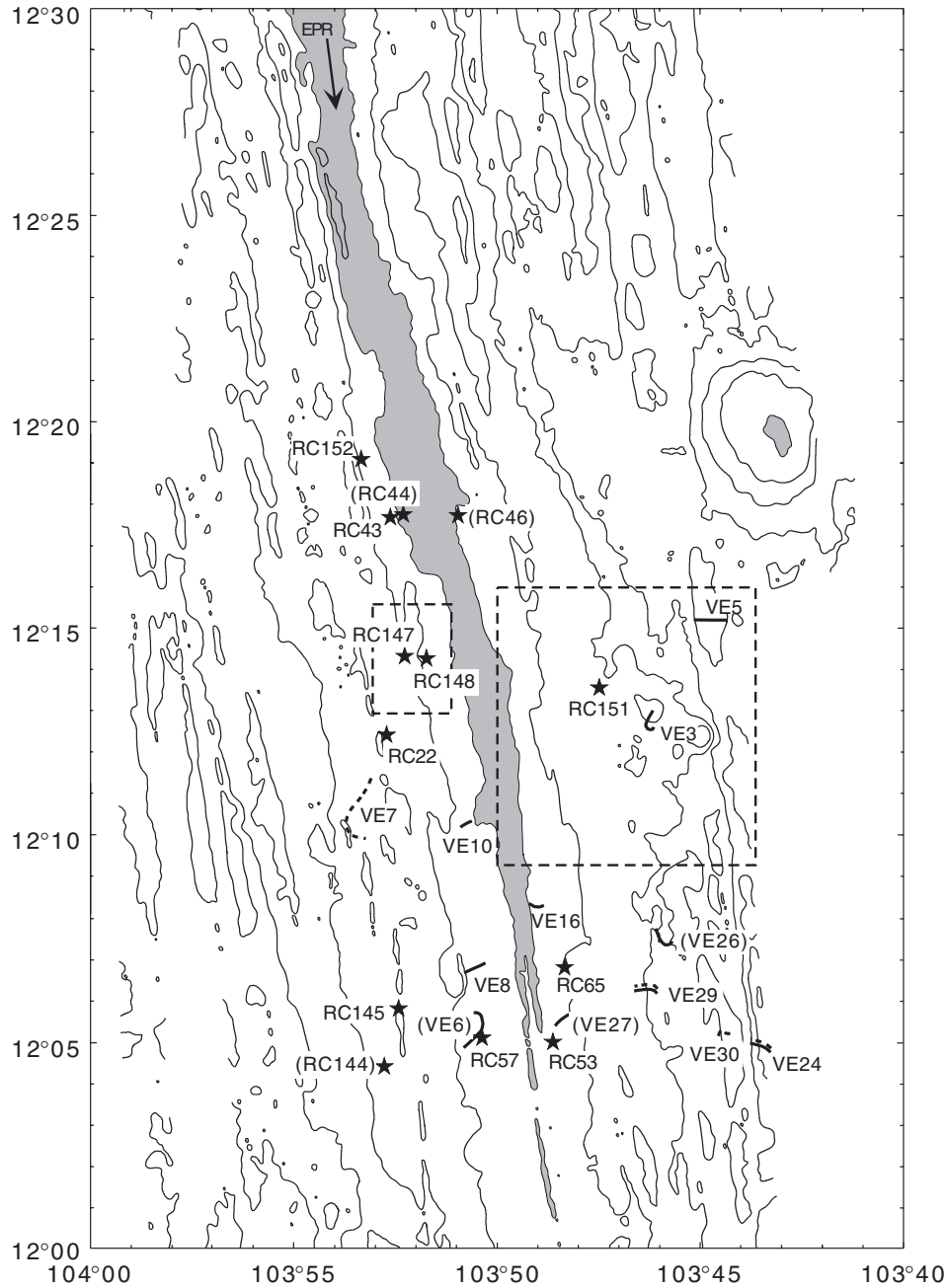


Figure 1. Bathymetric map of the East Pacific Rise, 12°00'–12°30'N. Bathymetric contour interval is 100 m [Monti *et al.*, 1987]. Regions shallower than 2700 m are shaded, highlighting the axis of the East Pacific Rise and the summit of an off-axis seamount. The locations of 21 depleted samples identified as off-axis eruptions (OA-NMORB) are shown as stars (rock cores) or solid lines (dredges). The six samples with names in parentheses have compositions “in between” the OA-NMORB and NMORB. Locations of four moderately enriched samples also believed to have erupted off axis (OA-TMORB) are shown as dashed lines (dredges). Dashed boxes indicate the locations of Figures 2a and 2b.

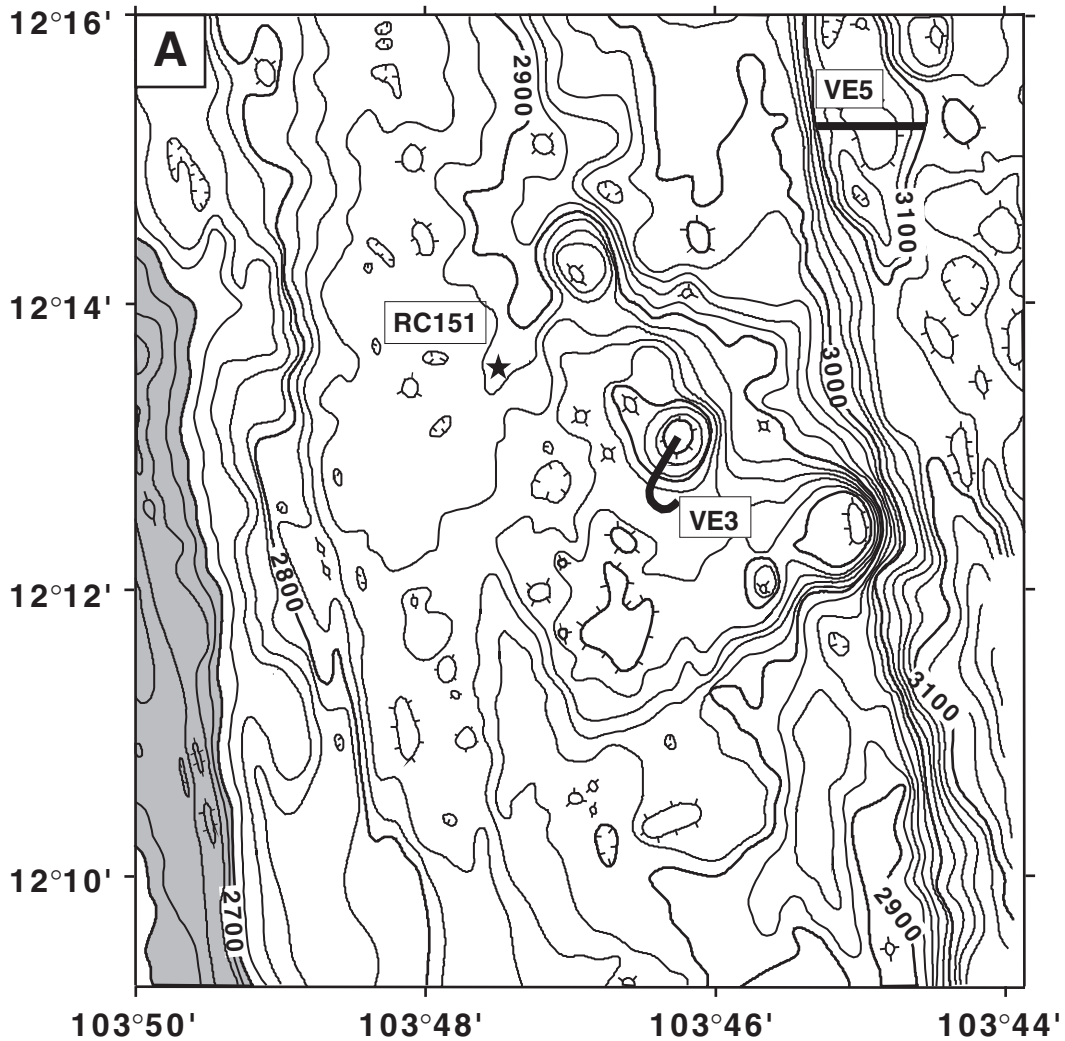


Figure 2. Examples of 12°N sample locations where the geology indicates off-axis eruptions, as discussed in the text. (a) Bathymetric map at 20 m contour interval [Monti *et al.*, 1987]. The shaded region shallower than 2700 m is centered on the EPR axis. The samples shown here have the petrological signature of OA-NMORB. The locations of VE3 and RC151 are areas of off-axis flows and seamount construction. (b) SeaMARC I side-looking sonar image of the seafloor west of the EPR, 12°13'–12°15'N. The locations of all three samples from this area are shown. RC149 is a typical NMORB, while RC147 and RC148 are OA-NMORB. The geology is discussed in the text.

ponder. This precise positioning allows much better constraints to be placed on the spatial systematics of the basalts.

[15] Several geological data sets exist for the 12°N region: multibeam bathymetry [Monti

et al., 1987], SeaMARC I sonar images of the region around the axis [Crane, 1987], and seafloor photographs from several camera tows during our study [Reynolds, 1995]. The navigation for these data has all been tied to the GPS-navigated bathymetric map.

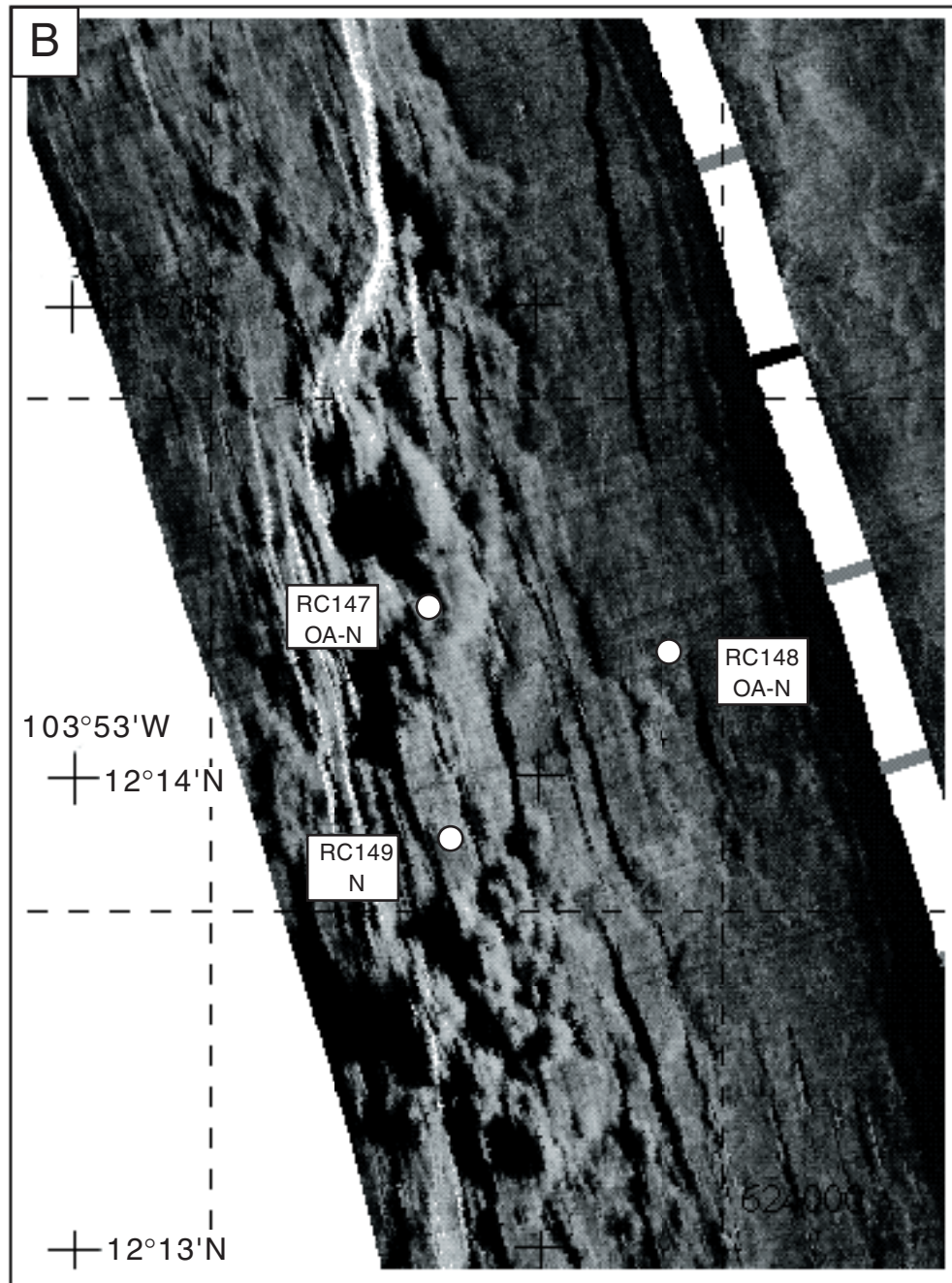


Figure 2. (continued)

A number of the dredges and rock cores sampled flows that can be identified as off-axis eruptions from the geological data.

[16] VE3 comes from a cluster of small cones 20–100 m high, east of the EPR axis at 12°13'N. Since cones do not form on the axis



itself, these must represent off-axis eruptions. RC151 is from the unusually flat terrain surrounding those cones, which appears to have been smoothed by off-axis lava flows that have covered abyssal hills in this region (Figure 2a).

[17] Faulting around the EPR does not begin closer than 0.5 km to the ridge axis, so flows that cover faults must have either traveled some distance from vents at the axis or actually erupted from off-axis vents. RC147 is from a volcanic mound constructed on top of a fault zone and represents eruptions from an off-axis vent (Figure 2b). RC148 is from a region of lower acoustic reflectivity that appears to be a young flow with light sediment draping an outward facing fault (Figure 2b). VE8 and RC152 come from 100 m long pillow ridges aligned along off-axis fissures. Another possible example is dredge VE27, crossing a flow that partly covers a fault (Figure 1).

[18] The samples described in the preceding paragraphs are normal mid-ocean ridge basalt (NMORB), but TMORB can also erupt off axis. West of the axis at $12^{\circ}17' - 12^{\circ}18'$ is a (fault-bounded?) plateau covered by young, glassy sheet flows and the remains of collapsed lava lakes, nearly sediment-free, as seen in a camera tow. The TMORB sample RC42 ($K_2O/TiO_2 = 0.132$) comes from this terrain ($12^{\circ}17.62'N$, $103^{\circ}52.95'W$). However, for reasons outlined in section 4, the petrological discussion will focus on the NMORB.

4. Geochemical Characteristics of Off-Axis Samples

[19] The glasses from the $12^{\circ}N$ samples have been analyzed by electron microprobe and by direct current plasma spectrometry (DCP) at Lamont-Doherty Earth Observatory (Tables 1, 2, and 3). Additional DCP analyses were done at sea, and the Ba and Sr from those analyses are also used (Table 2). The MORB glass standard

JDF-D2 was used to calibrate both microprobe and DCP analyses and ensures that the two data sets are compatible.

[20] The $12^{\circ}N$ data set is representative of MORB compositions along the entire northern EPR, with a mean composition that is virtually identical to the mean for the northern EPR as a whole [Langmuir *et al.*, 1992] and a range in composition that encompasses the entire EPR, with the exception of some highly fractionated lavas that have been recovered from some ridge offsets. Hence the data set can be used to define the overall petrological characteristics and systematics of EPR volcanism [Reynolds *et al.*, 1992; Reynolds, 1995]. The MgO concentrations in $12^{\circ}N$ glasses range between 6.42 and 9.04% MgO. The data set includes 119 NMORB, 25 TMORB, and 1 EMORB. (NMORB have $K_2O/TiO_2 \leq 0.090$, equivalent to $Sr \leq 130$ ppm, $Ba/TiO_2 \leq 9.0$, $Ce/Yb \leq 0.95$, and $Ce/Sm \leq 0.83$. The TMORB from $12^{\circ}N$ have K_2O/TiO_2 up to 0.205. The EMORB has $K_2O/TiO_2 = 0.349$.)

[21] The recognition from geological evidence of basalts erupted off axis enables a comparison with the compositions of lavas erupted in the axial graben/axial fissure zone. This comparison requires a clear understanding of the chemical systematics of axial EPR basalts, which can be briefly systematized as follows. A primary control on chemical variations is low-pressure fractionation, which leads to the covariations of most elements with MgO. We remove this effect as much as possible by normalizing the data to 7.3% MgO, which is the mean for a large population of EPR lavas. (See the appendix for discussion of the normalizing parameters.) A second source of chemical variations in EPR lavas is the variation in parental magmas between NMORB and TMORB. Langmuir *et al.* [1992] showed that the "local variation" of the EPR for both major and trace elements is controlled by mixing

Table 1. Sample Locations^a

Sample	Depth, m	Latitude, °N	Longitude, °W	Distance From Axis, km	Geological Evidence for Off-Axis Eruption
<i>Depleted OA-NMORB</i>					
VE3–A,B	2780	12°13.2′	103°46.5′	7.04	yes
VE5–A	3110	12°15.2′	103°44.3–45.2′	10.37	
VE8–A,B	2770	12°6.7–7.0′	103°50.9–50.1′	–2.22	yes
VE10	2740	12°10.2–10.5′	103°51.0–50.7′	–2.09	maybe
VE24–A,B	3060	12°4.70–5.00′	103°43.23–43.80′	10.09	
VE29–A,C	2890	12°6.27–6.28′	103°46.12–46.55′	5.19	
RC22	2840	12°12.46′	103°52.60′	–4.41	
RC43	2730	12°17.71′	103°52.60′	–1.48	
RC53	2750	12°05.05′	103°48.44′	0.91	
RC57	2745	12°05.16′	103°50.35′	–2.32	
RC65	2790	12°06.77′	103°48.29′	1.85	
RC145	2800	12°05.85′	103°52.40′	–5.93	
RC147	2810	12°14.35′	103°52.25′	–3.06	yes
RC148	2765	12°14.29′	103°51.71′	–2.13	yes
RC151	2890	12°13.60′	103°47.47′	5.19	yes
RC152	2765	12°19.06′	103°53.12′	–2.22	yes
<i>“In Between” OA–NMORB and NMORB</i>					
VE6	2750	12°4.8–5.7′	103°50.9–50.6′	–2.69	
VE26	2900	12°7.45–7.75′	103°45.6–46.1′	6.30	
VE27–C	2780	12°5.70–5.52′	103°48.18–48.57′	1.30	yes
RC44	2685	12°17.80′	103°52.30′	–0.93	
RC46	2705	12°17.80′	103°50.98′	0.93	
RC144	2805	12°04.40′	103°52.80′	–6.95	
<i>OA–TMORB</i>					
VE7–A	2850	12°11.5–9.9′	103°53.1′	–6.48	
VE24–D	3060	12°4.70–5.00′	103°43.23–43.80′	10.09	
VE29–B	2890	12°6.27–6.28′	103°46.12–46.55′	5.19	
VE30	2875	12°5.24–5.29′	103°44.52–44.24′	8.57	

^aLocations of dredges and rock core samples in the 12°00′–12°30′N study area are shown. All samples were collected on the Venture leg 2 cruise in 1989. VE samples are dredges; RC samples are rock cores. The depleted OA-NMORB are defined in the text. They are interpreted as a characteristic magma type erupted off axis, independent of the axial magma chamber, with affinities to seamount lavas. The transitional OA-TMORB are tentatively identified as moderately enriched equivalents of the OA-NMORB. The distance of sample locations to the ridge axis (i.e., the axial graben) is measured along flow lines perpendicular to the axis. Positive distances are to the east; negative distances are to the west.

between the relatively enriched TMORB and the more depleted NMORB. A third source of chemical variation for EPR lavas has been identified by Reynolds *et al.* [1992] and further discussed by Langmuir *et al.* [1992]. It is reflected in covariations of most major elements as well as trace elements at constant 7.3% MgO and has major influence on the composition of the NMORB [Reynolds,

1995]. The clearest signal is in the positively correlated covariations in TiO₂ and FeO*, and hence we named this signal “TiFe_{7.3}” [Reynolds *et al.*, 1992].

[22] There is strong evidence for the involvement of plagioclase in creating the TiFe_{7.3} signal, most notably a negative Sr anomaly that is correlated with increasing TiFe_{7.3} [Reynolds,



Table 2. Microprobe and Shipboard DCP Analyses^a

Sample	N	SiO ₂	TiO ₂	Al ₂ O ₃	FeO*	MnO	MgO	CaO	Na ₂ O	K ₂ O	P ₂ O ₅	Sum	Mg Number	TiFe _{7.3}	K ₂ O/ TiO ₂ Probe	K ₂ O/ TiO ₂ DCP	Sr	Ba/ TiO ₂
<i>OA-N-MORB</i>																		
VE3-A	8	50.51	1.43	14.52	10.38	0.18	7.82	12.18	2.44	0.07	0.18	99.75	59.3	-0.31	0.047	0.050	95	4.18
VE3-B	5	50.71	1.04	14.68	9.41	0.18	8.53	12.79	2.16	0.03	0.18	99.76	63.7	-0.47	0.030	0.036	71	3.82
VE5-A	6	50.58	1.47	14.38	10.61	0.18	7.62	12.13	2.71	0.07	0.12	99.91	58.1	-0.48	0.045	0.044	102	3.61
VE8-A	11	50.75	1.63	14.33	10.69	0.20	7.38	11.70	2.81	0.09	0.19	99.81	57.2	-0.70	0.055	0.052	102	4.83
VE8-B	17	50.61	1.36	14.65	9.89	0.20	8.15	12.14	2.47	0.07	0.16	99.73	61.4	0.10	0.054	0.053	99	4.47
VE10	20	50.84	1.50	14.32	10.57	0.19	7.65	11.82	2.57	0.08	0.18	99.78	58.4	-0.38	0.054	0.039	101	4.36
VE16	7	50.51	1.49	14.31	10.80	0.20	7.73	11.77	2.51	0.09	0.18	99.63	58.1	0.00	0.059	0.051	103	4.50
VE24-A	12	50.73	2.04	13.38	13.19	0.23	6.44	10.48	2.93	0.10	0.20	99.76	48.6	0.16	0.048	0.049	97	4.19
VE24-B	5	50.69	1.56	14.14	11.24	0.24	7.38	11.51	2.71	0.08	0.20	99.78	56.0	-0.26	0.054	0.051	93	3.63
VE29-A	9	50.91	1.76	13.94	11.38	0.22	7.10	11.43	2.73	0.11	0.20	99.82	54.7	-0.48	0.064	0.059	98	5.66
VE29-C	11	50.52	0.99	14.87	9.22	0.18	8.54	13.13	2.12	0.04	0.14	99.80	64.2	-0.73	0.043	0.046	72	3.41
RC22	5	50.69	1.56	14.47	10.43	0.21	7.71	11.89	2.54	0.09	0.19	99.82	58.9	-0.31	0.055			
RC43	5	51.02	1.46	14.35	10.12	0.17	7.69	12.00	2.69	0.10	0.19	99.82	59.5	-0.82	0.069			
RC53	6	50.81	1.56	14.16	10.90	0.19	7.48	11.56	2.72	0.09	0.15	99.65	57.0	-0.37	0.057		103	4.33
RC57	5	50.30	1.39	14.48	10.10	0.16	7.94	12.37	2.58	0.06	0.19	99.61	60.3	-0.42	0.046		97	4.31
RC65	5	50.69	1.45	14.37	10.24	0.18	7.82	12.14	2.62	0.08	0.20	99.83	59.7	-0.42	0.053		98	4.07
RC145	5	51.00	1.69	13.87	11.03	0.20	7.33	11.78	2.55	0.12	0.19	99.78	56.3	-0.38	0.068		98	4.57
RC147	8	50.84	1.43	14.51	10.12	0.19	7.78	12.20	2.52	0.07	0.17	99.87	59.8	-0.68	0.052			
RC148	5	50.99	1.39	14.40	10.34	0.18	7.77	12.10	2.41	0.09	0.19	99.89	59.2	-0.55	0.062			
RC151	5	50.29	1.09	14.95	9.36	0.16	8.45	12.94	2.37	0.05	0.18	99.88	63.6	-0.60	0.047		79	4.38
RC152	9	50.79	2.01	13.90	11.93	0.21	6.63	11.08	2.91	0.12	0.22	99.85	51.8	-0.67	0.060		108	4.67
<i>"In Between" OA-NMORB and NMORB</i>																		
VE6	12	51.10	2.00	13.66	11.78	0.21	6.90	11.18	2.65	0.12	0.19	99.82	53.1	-0.19	0.058	0.061	98	5.15
VE26	7	50.72	1.83	14.02	11.50	0.20	7.06	11.39	2.68	0.10	0.21	99.76	54.3	-0.33	0.056	0.062	104	5.02
VE27-C	9	50.52	1.38	14.89	9.71	0.19	8.10	12.14	2.52	0.08	0.19	99.76	61.7	-0.16	0.058	0.060	111	5.27
RC44	5	50.87	1.93	13.72	11.76	0.22	6.90	11.18	2.77	0.12	0.21	99.73	53.2	-0.32	0.061		106	5.26
RC46	5	50.80	1.97	13.86	11.75	0.21	6.94	11.11	2.74	0.14	0.21	99.76	53.3	-0.18	0.069		102	5.04
RC144	5	50.70	1.97	13.76	12.03	0.22	6.78	11.10	2.84	0.12	0.20	99.77	52.2	-0.29	0.063		99	4.97
<i>OA-TMORB</i>																		
VE7-A	7	50.44	1.64	14.84	9.74	0.18	7.65	12.18	2.85	0.19	0.18	99.93	60.3		0.118	0.107	156	13.3
VE24-D	9	50.43	2.15	14.39	10.97	0.21	6.49	10.91	3.43	0.45	0.27	99.74	53.4		0.211	0.205	170	18.8
VE29-B	11	50.63	1.62	14.76	10.01	0.18	7.29	12.09	2.86	0.15	0.18	99.80	58.5		0.094	0.092	143	10.5
VE30	12	50.61	2.04	14.47	10.59	0.20	6.61	11.11	3.37	0.47	0.25	99.77	54.7		0.232	0.192	169	20.1
JDF-D2 standard		50.8	1.89	13.8	12.17	0.22	6.83	10.8	2.77	0.215	0.230	99.73	52.1	0.15	0.114	0.114	116	11.8
Precision		0.25	0.04	0.13	0.18	0.03	0.13	0.13	0.10	0.03	0.02			0.29	0.05	2.83 ^b	4.6 ^b	0.26 ^b



1995]. There is no correlation with geochemical indicators of enrichment or with radiogenic isotope compositions, so $\text{TiFe}_{7.3}$ appears to be unrelated to mantle source composition. Because plagioclase is stable in MORB systems only at crustal and very shallow mantle pressures, the $\text{TiFe}_{7.3}$ signal must originate at that level and not in the mantle source composition or the melting process. As will be seen below and in Figure 4, there is no evidence of the process that produces high values of $\text{TiFe}_{7.3}$ in off-axis lavas; therefore we believe that this process is limited to the axial magma system. An in-depth discussion of the $\text{TiFe}_{7.3}$ process and its implications is beyond the scope of this paper and will instead be the subject of a separate publication.

[23] In exploring the existence of a unique off-axis composition this entire complex spectrum of axial compositions and petrological systematics needs to be considered. Because the geochemical enrichment in TMORB can be such a dominant influence, the following discussion of the off-axis geochemical signature first focuses on the NMORB alone. TMORB are discussed in sections 5 and 7 in conjunction with seamount lavas.

[24] The chemical compositions of the depleted basalts erupted off axis (solid triangles) are compared to NMORB from the 12°N ridge axis in Figures 3 and 4. The samples erupted off axis have lower FeO^* and TiO_2 and higher CaO at the same MgO content. They also have lower Ba and other incompatible trace element contents and occupy distinct fields on plots of

$\text{Na}_{7.3}$ versus $\text{TiFe}_{7.3}$ and Sr versus $\text{TiFe}_{7.3}$. Thus there is a clear distinction between the NMORB lavas erupted on an off axis in the 12°N region.

[25] This distinction is complicated by the temporal zonation that exists in the 12°N region [Reynolds *et al.*, 1992]. Older, more sedimented lavas at 12°N have lower $\text{TiFe}_{7.3}$ than younger lavas, and this difference is in the same overall direction as the on- to off-axis distinction. An additional line of evidence, however, suggests that the chemical distinctiveness of lavas erupted off axis is not related to this temporal change.

[26] NMORB samples were recovered along the EPR axis from 8°N to 14°N during the Chemistry of the East Pacific Rise (CHEPR) cruise of the R/V *New Horizon* in April 1985, [Langmuir *et al.*, 1986; Langmuir, 1988]. These samples reflect at zero age the entire range of $\text{TiFe}_{7.3}$ that erupts over time at 12°N . Because those data are from the same laboratory and calibrated to the same standards as the 12°N analyses, a precise comparison is possible. We have selected only those CHEPR dredges with a dredge track entirely within 1 km of the axial summit trough, in order to avoid any possible off-axis flows that may have been sampled inadvertently. (One axis sample is excluded, CH99.1, discussed further below.) The fields of those data are circled in Figures 3 and 4, and they include the full range of low to high $\text{TiFe}_{7.3}$ found along the EPR. The off-axis-type samples from 12°N do not fall on the

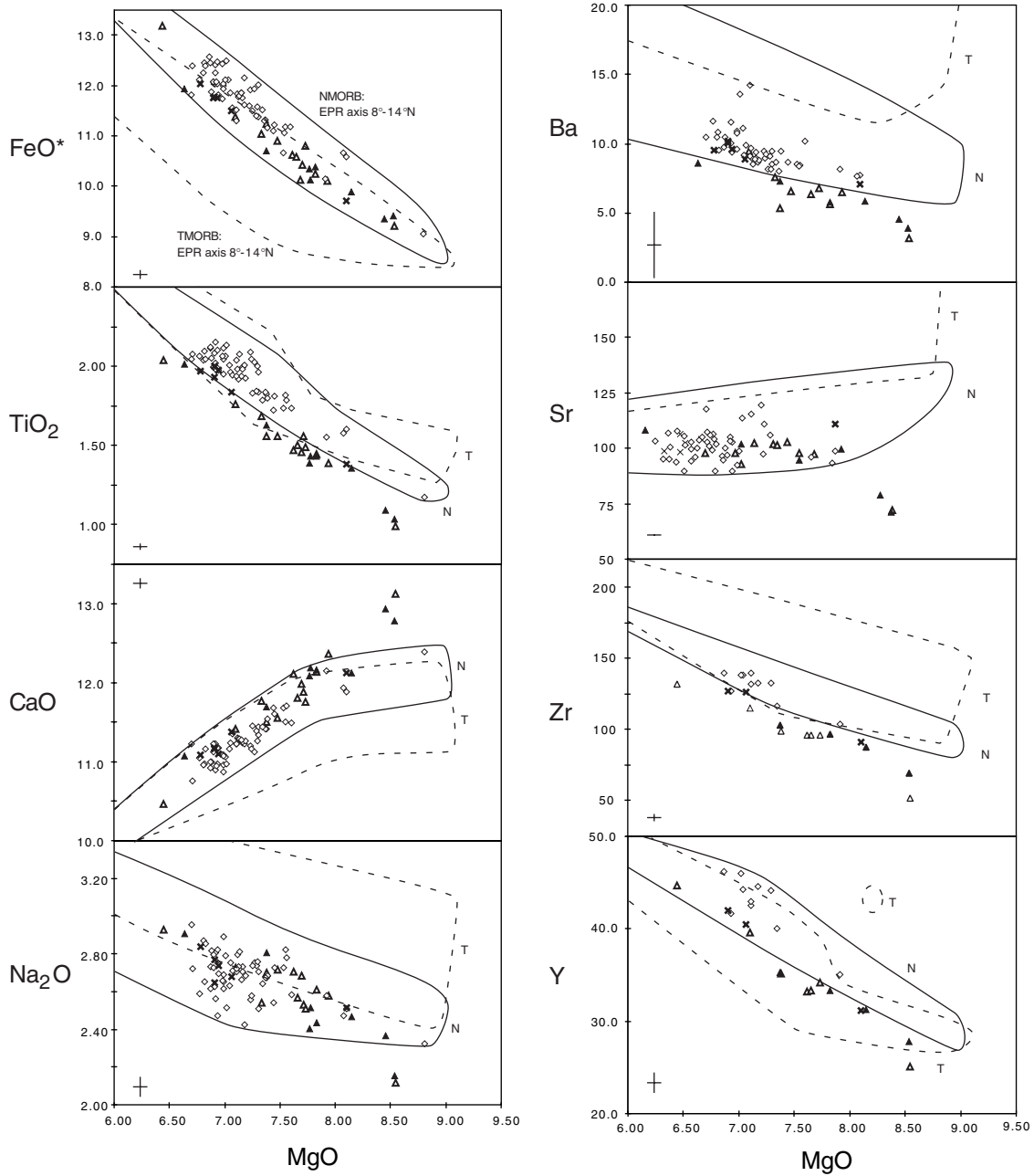
Notes to Table 2:

^aCompositions of samples identified as off-axis eruptions in the 12°N study area are shown. Microprobe analyses were done at Lamont-Doherty Earth Observatory. Counting times were 30 s for Na_2O and K_2O and 20 s for the other oxides. Corrections were applied to the data to remove errors associated with poor sums and to normalize all analyses to the JDF-D2 glass standard (details are given by Reynolds and Langmuir [1997]). The data here are averages of *N* individual analyses. Mg number was calculated assuming $[\text{Fe}^{2+} = 0.93\text{Fe}^{\text{total}}]$. $\text{TiFe}_{7.3}$ is calculated only for depleted samples that appear to lie on an olivine-plagioclase-clinopyroxene cotectic (see also caption for Figure 3). Trace elements: Sr and Ba/TiO_2 in handpicked glass, analyzed by direct current plasma spectrometer (DCP) at sea during the Venture cruise. Precision is to 2 standard deviations of a five-point average.

^bPrecision to 2 standard deviations.



- ◇ 12°N NMORB <1km from axis
- × in between NMORB and OA-NMORB
- ▲ 12°
- △ 12°N other OA-NMORB





field of EPR NMORB, nor do they fall along the NMORB/TMORB trend defined by lavas from the ridge axis. In comparison to the entire EPR zero-age data set, the 12°N samples for which there is geological evidence for eruption off axis (solid triangles) plot in distinct fields.

[27] The distinctive signature of the off-axis type includes the combination of low $\text{TiFe}_{7.3}$ with lower $\text{Na}_{7.3}$, $\text{Al}_{7.3}$, and Sr and incompatible trace elements than is found in the axis samples. The most incompatible elements, $\text{Ba}_{7.3}$, $\text{K}_{7.3}$, and $\text{P}_{7.3}$, exhibit almost no overlap with axis samples (Figures 3 and 4). Thus the combination of major and trace elements shows that the off-axis type is not a subset of lavas from the EPR axis. We refer to this distinct off-axis type as off-axis NMORB, or OA-NMORB.

[28] The clearest contrast between NMORB and OA-NMORB can be seen when the positions on multiple plots are combined to form a single off-axis discriminant value (Figure 5). A single, linear discriminant based on only major elements from microprobe data is not adequate, but one based on both major and trace elements (Figure 5) provides a means of distinguishing samples erupted from the 12°N axial magma system and those from independent, off-axis magma systems, even in the absence of geological information. The discriminant uses the correlations between $\text{TiFe}_{7.3}$ and $\text{Na}_{7.3}$, $\text{Al}_{7.3}$, Sr, etc., defined by the axis-type 12°N NMORB data. For each sample the discriminant is the sum of offsets from lines

representing these correlations. The lines are determined by least squares fits to up to 87 samples, depending on the element. The off-sets can be positive or negative; OA-NMORB have negative offsets from each of these correlation lines. This discriminant reinforces the conclusion that the OA-NMORB are a distinct magma type and also provides a clear means of classifying other samples for which the geological constraints are either ambiguous or unknown.

[29] All samples identified from the geological data as having erupted off axis are either OA-NMORB or some variety of TMORB. The eight OA-NMORB identified by geological evidence are shown by the solid triangles in Figures 3 and 4. Four of these have trace element data, and their discriminant values are included in Figure 5. Thirteen samples are identified as OA-NMORB on the basis of composition alone and are the open triangles in Figures 3 and 4. Seven of these have trace element data and are shown in Figure 5. Six additional samples, labeled with crosses in Figures 3 and 4, are intermediate in composition. In total, 27 out of 58 total depleted samples, or 46%, recovered from off-axis terrain in the 12°N region are likely OA-NMORB. In contrast, none of the samples recovered on axis pass as the OA-NMORB discriminant.

[30] The discriminant also helps us investigate the entire CHEPR data set to determine how many OA-NMORB samples were recovered in the earlier dredging expedition. A search

Figure 3. Lavas erupted off axis in the 12°00′–12°30′N region, compared with on axis EPR NMORB from 8° to 14°N. Solid triangles, 12°N lavas erupted off axis, as determined from geological evidence; open triangles, 12°N lavas with the same off-axis petrological characteristics (OA-NMORB); crosses, 12°N lavas with composition intermediate between OA-NMORB and NMORB; open diamonds, 12°N NMORB samples located within 1 km of the axial graben; circled fields, NMORB (solid lines) and TMORB (dashed lines) from the EPR axis 8°–14°N, limited to those located within 1 km of the axial graben, from dredges of *Langmuir et al.* [1986, 1988] and from the 12°N region. Sample CH99.1 is on axis but is omitted (see text). Error bars represent 2-sigma analytical precision.

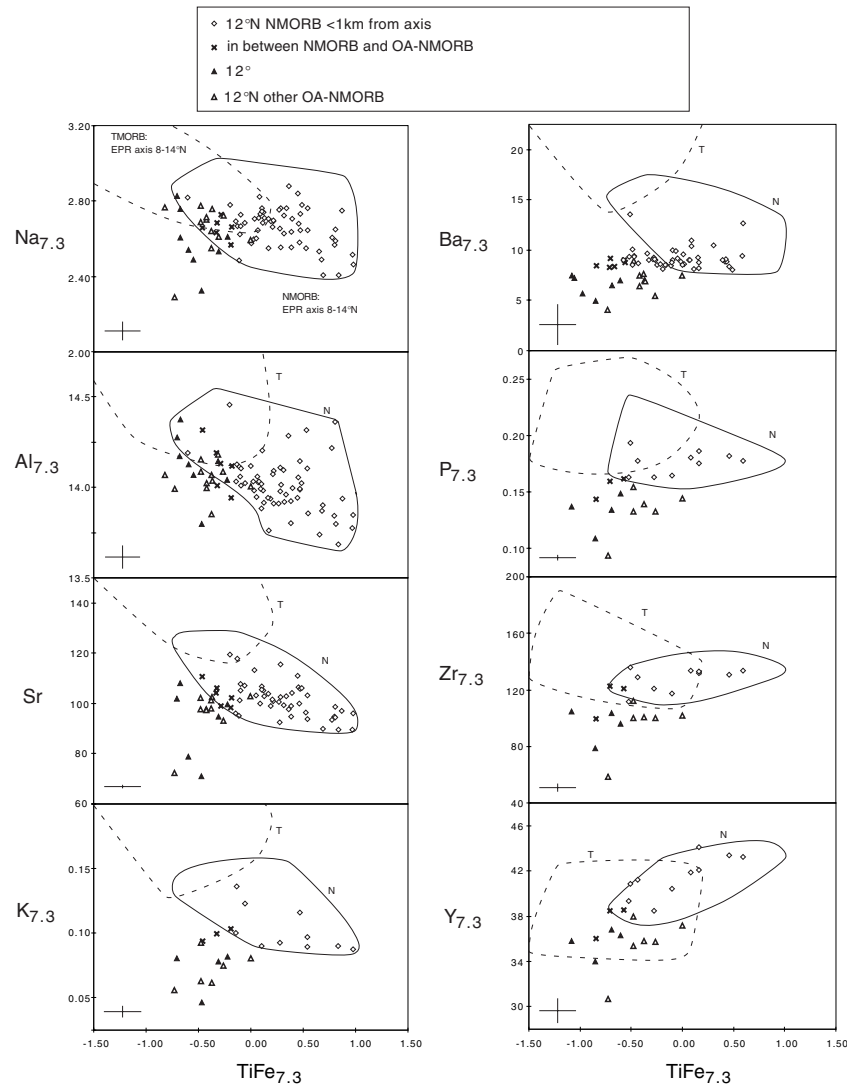


Figure 4. Lavas erupted off axis in the $12^{\circ}00' - 12^{\circ}30'N$ region, compared with on-axis EPR NMORB from 8° to $14^{\circ}N$, as in Figure 3. Symbols are as in Figure 3. The compositions have been corrected for low-pressure fractionation to 7.3% MgO, as described in the appendix. The variations in on-axis NMORB are dominated by $TiFe_{7.3}$ systematics, so the comparison with off-axis lavas is most effective when those $TiFe_{7.3}$ variations are taken into account. These plots show that the off-axis magma type does not fall along the NMORB-TMORB continuum of axis lavas and is instead offset below those data. Major elements are from microprobe analyses; Ba and Sr are from DCP analyses both at sea and at Lamont; and the other trace elements are from DCP analyses at Lamont only. Error bars represent 2 sigma analytical precision. Major element oxide corrections have the form $[C_i + (MgO - 7.3)b]$, where C_i refers to the measured concentration in the sample. $TiFe_{7.3} = [(Fe_{7.3} - 11.16) + 1.5(Ti_{7.3} - 1.9)]$. Slopes b : $FeO^* = 1.8$; $Al_2O_3 = 0.71$. Minor and trace element corrections have the form $[C_i(1 - F_{7.3})^{(1 - D)}]$. $F_{7.3} = \{-1.6413[(MgO - 7.3)/7.3]^2 + 1.8732\{\text{abs}[(MgO - 7.3)/7.3]\} \text{sign}(7.3 - MgO)\}$. Bulk distribution coefficients D : $TiO_2 = 0.14$; $Na_2O = 0.69$; $Ba = 0.00007$; $K_2O = 0.001$; $P_2O_5 = 0.092$; $Zr = 0.47$; $Y = 0.16$.



of the 123 CHEPR dredges from 5° to 14°N along the EPR [Langmuir *et al.*, 1986; Langmuir, 1988] reveals only eight samples from seven dredges that fit the criteria. Three of these have trace element data (Figure 5). The geological settings of all but one of these eight dredges are consistent with the samples having erupted off axis. Two are from dredges deliberately located well off axis (CH101.3 at 10°12.6'N; CH102.1 at 10°15.9'N). One is from a dredge 3 km east of the axis (CH46.1 at 10°27.8'N). Another is from a dredge that started 4 km off axis and crossed over the EPR summit (CH11.2 at 13°12.2'N). Two more are from a cone next to the ridge axis at 12°22'N (CH119.1, CH119.3), and one is from a dredge at the eastern tip of the 11°45' overlapping spreading center (OSC) that crossed a small cone east of the axis (CH35.4). The one OA sample dredged from the EPR axis is from 10°9.8'N (CH99.1), the curving tip of the axis at the western intersection with the Clipperton Transform. This location can be regarded as an along-strike edge of the melt supply for the ridge axis, similar to the across-strike setting of the off-axis eruptions.

5. Relationship to Near-Ridge Seamounts

[31] The OA-NMORB samples have no counterpart along the axis of the EPR (except one sample at a ridge-transform intersection), but they strongly resemble many depleted basalts from seamounts near the EPR. For this comparison we consider seamount glasses with the same range of MgO as occurs among the 12°N OA-NMORB. In addition, because the OA-NMORB magma type is defined only for depleted compositions, we sort the seamount data to exclude enriched samples. EPR NMORB and TMORB are normally distinguished using incompatible trace element characteristics, e.g., K₂O/TiO₂. How-

ever, EPR TMORB also have distinctive major element characteristics that strongly correlate with the degree of trace element and isotopic enrichment [Sinton *et al.*, 1991; Langmuir *et al.*, 1992; Reynolds, 1995]. The TMORB have higher Al₂O₃ and Na₂O at all MgO levels. They have lower SiO₂ and CaO, especially in less evolved lavas, and distinctly lower FeO*, especially in more evolved lavas. This combination of major element characteristics can be used as an alternative means of identifying enriched compositions.

5.1. Assorted Near-EPR Seamounts

[32] For comparison with the OA-NMORB, we have combined several seamount data sets published by Batiza and Vanko [1984], Batiza *et al.* [1989], Allan *et al.* [1994], and Niu and Batiza [1997, 1998]. Their glass analyses by electron microprobe at the Smithsonian Institution have been adjusted by the known difference between Smithsonian VG-2 and Lamont JDF-D2 microprobe calibrations, so that the analyses can be directly compared with our data (Figure 6). The Lamont Seamounts are excluded from the initial comparison and discussed in section 5.2. Of the remaining 122 near-EPR seamount samples in the appropriate MgO range, 51 have “depleted” K₂O/TiO₂ ratios (<0.090). However, when the seamount data are also sorted according to the major element systematics, using the data fields of NMORB and TMORB from the EPR axis for reference, 29 of the seamount samples with trace element criteria of NMORB, or approximately half, have major element compositions in the TMORB fields (Figure 7). This is not expected if seamount melts are produced in the same way and from the same range of mantle source compositions as EPR melts, in which the major and trace element characteristics of enriched versus depleted lavas are strongly correlated. An explanation for the seamount

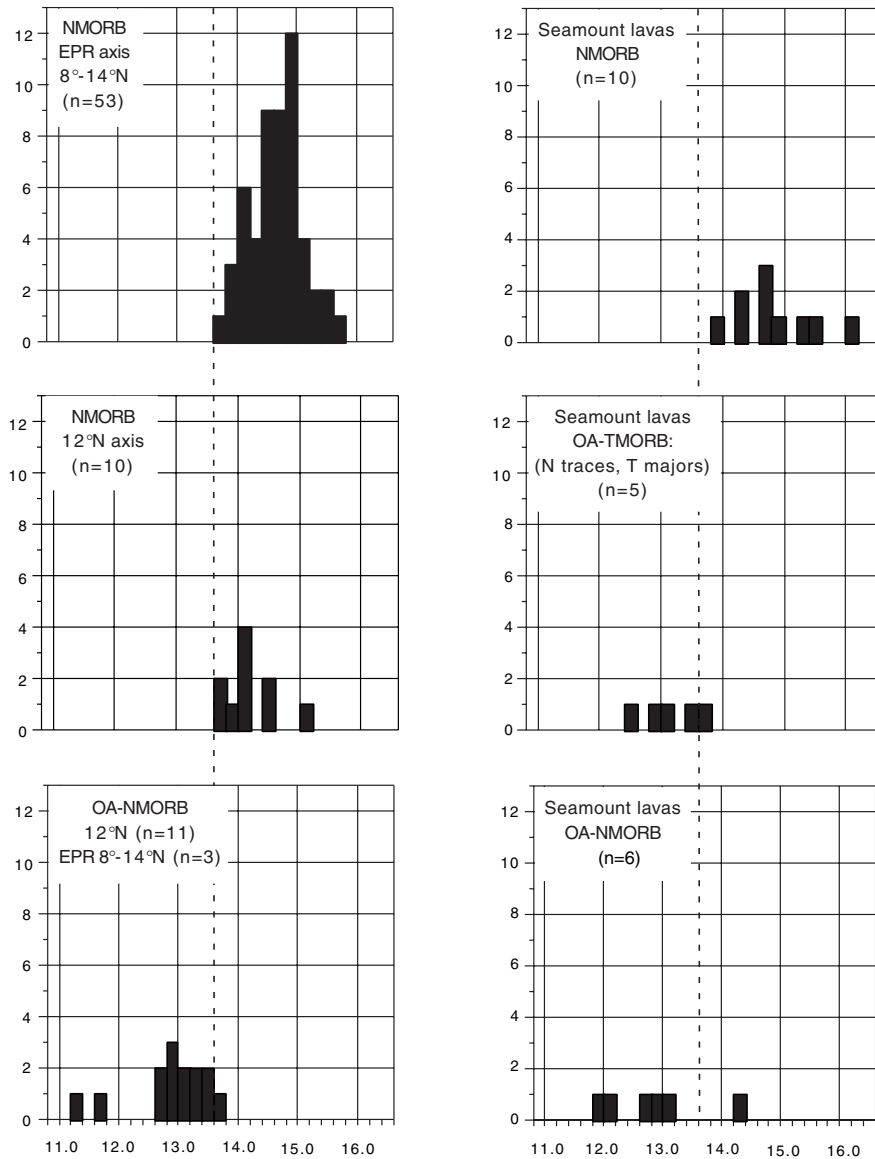


Figure 5. Histograms displaying compositional differences between the OA-NMORB at 12°N, NMORB axis lavas from the same region, and NMORB axis lavas from the EPR 8°–14°N. The discriminant incorporates both major and trace elements, as described in the text, so only samples with full major and trace element analysis are used. The dashed lines indicate the boundary between OA-NMORB and NMORB. The data plotted here are limited to samples with high-quality trace element data on glasses, from DCP or inductively coupled plasma-mass spectrometry (ICP-MS). Discriminant $X = [(Na_{7.3}/2.68) + (Al_{7.3}/14.04) + (Sr/104) + (Ba_{7.3}/9.8) + (K_{7.3}/0.104) + (P_{7.3}/0.170) + (Zr_{7.3}/122) + (0.428 TiFe_{7.3}) + 7.08]$. EPR axis data are from 8°–14°N as in Figures 3 and 4. The three OA-NMORB samples from the CHEPR data set that have DCP analyses are CH99.3, CH102.2, CH119.3. The EPR sample with discriminant value of 13.61 is CH119.3. Seamount data are from *Niu and Batiza* [1997, 1998], discussed in section 5.1. The seamount sample with discriminant value of 14.28 is R94-2, with anomalously (erroneously?) high Ba value of 21.7 ppm.



data, by analogy to EPR basalt systematics, is that the mantle source of these lavas was mildly enriched but had lost a significant fraction of its incompatible trace element budget extracted as a low-degree melt before the seamount magmas were produced. We exclude those 29 samples as being from an enriched mantle source and discuss them separately. The remaining 22 seamount samples have both major and trace elements in the range of depleted EPR basalts. They are from Seamounts 1, 3, 4, 6, 8, D, N-2, and N-3, between 8°38'N and 13°00'N.

[33] This refined data set is remarkably similar to the OA-NMORB data from the 12°N region (Figures 6 and 7). Some seamount lavas provide even more extreme examples of the OA-NMORB characteristics. Several of them extend to even lower Sr, lower TiO₂, lower TiFe_{7.3}, and higher SiO₂. The OA-NMORB samples clearly have greater affinity to these seamount lavas than to NMORB from the ridge axis.

[34] The discriminant developed in section 4 can also be applied to these near-EPR seamount compositions. For this purpose, we are limited to those samples that have trace element analyses with a precision comparable to DCP, in this case the inductively coupled plasma-mass spectrometry (ICP-MS) data of *Niu and Batiza* [1997, 1998]. Their data are divided into samples with incompatible trace elements in the range of EPR NMORB and ones in the range of EPR TMORB. Those with NMORB-like trace elements are further divided into two groups, one with major elements in the range of NMORB, and a second with major elements in the range of TMORB. Discriminants calculated for these subsets of the seamount data are plotted separately in the histograms of Figure 5. Several points are evident. First, the discriminant does sort the seamount lavas into NMORB and OA-NMORB in the same way as for lavas recovered near or on the EPR.

Second, the middle right-hand plot, showing samples with NMORB-like trace elements and TMORB-like major elements, emphasizes that this discriminant is only applicable to samples in the NMORB compositional range. Those with TMORB-like major elements have elevated discriminant values because of higher Na_{7.3} and Al_{7.3} that are part of the major element signature of enriched lavas. We interpret these samples as possible OA-TMORB derived from enriched mantle; they should be compared with TMORB. Sorting them out of the NMORB data set is important for clarifying the systematics of seamount samples.

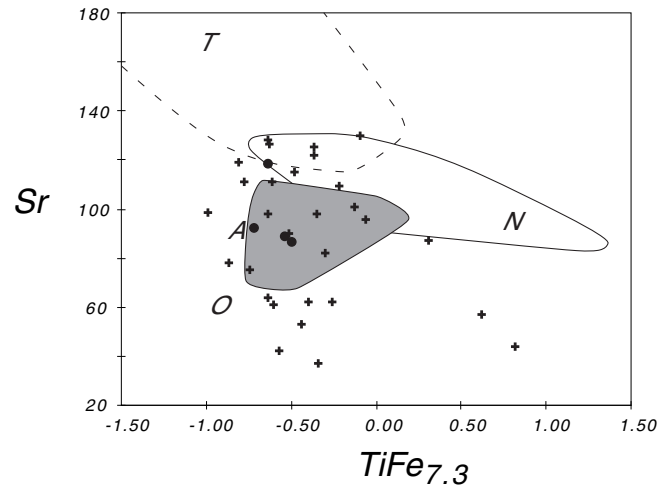
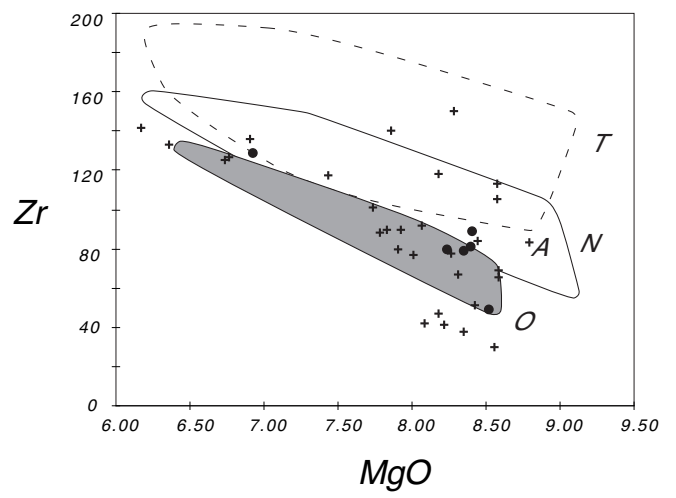
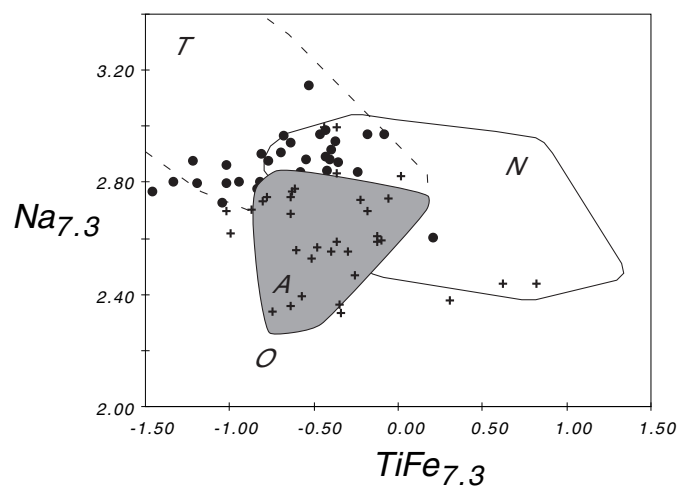
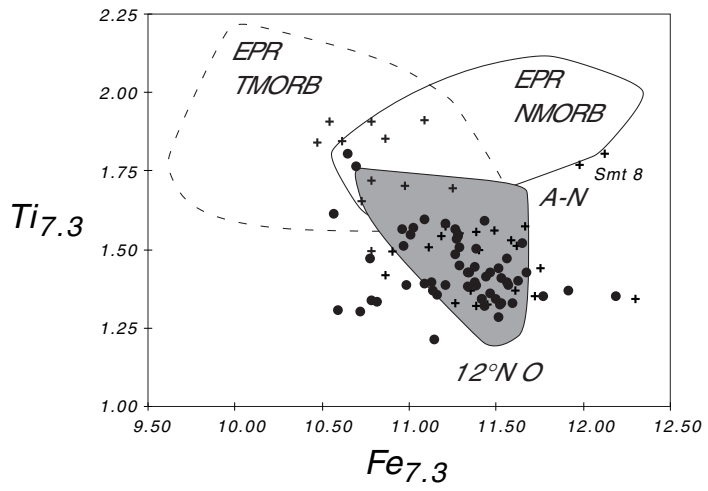
5.2. Lamont Seamounts

[35] The Lamont Seamounts at 10°N are considered separately. The larger volcanoes in this chain are the most extensively sampled and best studied of the near-EPR seamounts. Basalts from the Lamont Seamounts have been classified in the past as NMORB, and their average is more depleted in trace elements and has lower ⁸⁷Sr/⁸⁶Sr and higher ¹⁴³Nd/¹⁴⁴Nd than nearby EPR lavas [*Zindler et al.*, 1984; *Fornari et al.*, 1988; *Allan et al.*, 1989]. Of the glass analyses in the desired MgO range, 23 must be excluded owing to their major element compositions in the range of EPR TMORB, which leaves 74 samples remaining. These have low concentrations and low ratios of incompatible trace elements compared with EPR samples, including low TiO₂, Sr, Ce, Yb, La/Sm, and Ce/Yb. The reason for the relatively high Na_{7.3} is not known (Figures 6 and 8). Aside from the high Na_{7.3} the characteristics of depleted Lamont Seamount lavas are shared by the OA-NMORB.

[36] The major element systematics of the Lamont Seamounts may reflect an additional complication of source enrichment that appears to be correlated with the size of the seamount.



● Lamont seamounts and cones (N traces, N majors)
+ other near-EPR seamounts (N traces, N majors)





Of the 74 samples under consideration, 44 are from the 1 km high Lamont Seamounts (MIB, MOK, SASHA, DTD, NEW), and 30 are from 50–200 m high cones around the base of the large seamounts. OA-NMORB (solid circles in Figures 6 and 8) are widespread on both the large seamounts and the small cones. However, all but one of the 23 samples excluded above on the basis of TMORB-like major element characteristics are from the large seamounts. These samples are interpreted as OA-TMORB. This suggests that magmas supplied to these large seamounts have come from mantle that was originally moderately enriched, and more enriched than the source of the small cones. This has not been recognized previously because inferences about mantle source enrichment have been made on the basis of incompatible trace elements and radiogenic isotopes of incompatible trace elements. The origin of the Lamont Seamounts is clearly complex in detail, but many aspects of their chemical compositions are dominated by the OA magma type.

6. Origin of Off-Axis Magmas

[37] The similarity between depleted lavas erupted near the EPR axis and many of the depleted seamount lavas suggests that seamounts are only the largest and most obvious manifestation of off-axis volcanism. Volcan-

ism with chemical characteristics similar to seamounts is more widespread than would be inferred from morphology alone. This implies that the magmatic processes that give rise to this chemical type are not necessarily associated only with the substantial magma pulses that produce seamounts but, in fact, are more evenly distributed about the EPR axis. Seamounts, then, may be the most obvious bathymetric manifestation of what, in fact, is a more general and widespread phenomenon.

[38] The similarity to depleted seamount lavas also means that the extensive petrogenetic discussion of the origin of the chemical signature associated with seamounts applies to the OA-NMORB as well. Numerous discussions of trace element compositions have emphasized the concept that to first order, seamount magmas sample the same mantle sources as the EPR axis, except that individual seamount magma compositions span a wider range [e.g., Zindler *et al.*, 1984; Fornari *et al.*, 1988; Allan *et al.*, 1989; Niu and Batiza, 1997, 1998]. In this model, pooling of magmas in crustal reservoirs at the ridge axis leads to eruption of more homogeneous compositions on axis. A more recent concept, based on interpretations of major element data, is that seamount lavas are produced in the EPR melting regime, but interaction be-

Figure 6. Depleted basalts from seamounts near the EPR, compared with compositional fields of basalts from the EPR axis 8°–14°N. The fields of 12°N OA-NMORB are shaded. Solid circles, Lamont Seamounts and nearby cones, 10°N [Zindler *et al.*, 1984; Allan *et al.*, 1989]; plus symbols, other near-EPR seamounts [Batiza and Vanko, 1984; Allan *et al.*, 1994; Niu and Batiza, 1997, 1998]. Notice that the seamount samples overlap part of the EPR axis data field but scatter into and beyond the field of 12°N OA-NMORB. Seamount samples that have major element compositions like those of EPR TMORB have been excluded; see text and Figures 7 and 8. Two outliers from Seamount 8, dredge 10, labeled in the Ti_{7.3} versus Fe_{7.3} plot, resemble the EPR axis basalts. These samples are from a deep dredge that may have sampled surrounding seafloor (R. Batiza, personal communication, 1997). Electron microprobe compositions from the Smithsonian microprobe (VG-2 standard) have been adjusted to match Lamont microprobe calibrations (JDF-D2 standard), using the following coefficients [Reynolds, 1995]: 0.998 SiO₂, 0.988 Al₂O₃, 0.987 FeO, 1.047 MgO, and 1.019 Na₂O. Adjustments applied to microprobe data from Niu and Batiza's [1997, 1998] "new" VG-2 are 0.988 Al₂O₃ and 1.023 Na₂O.

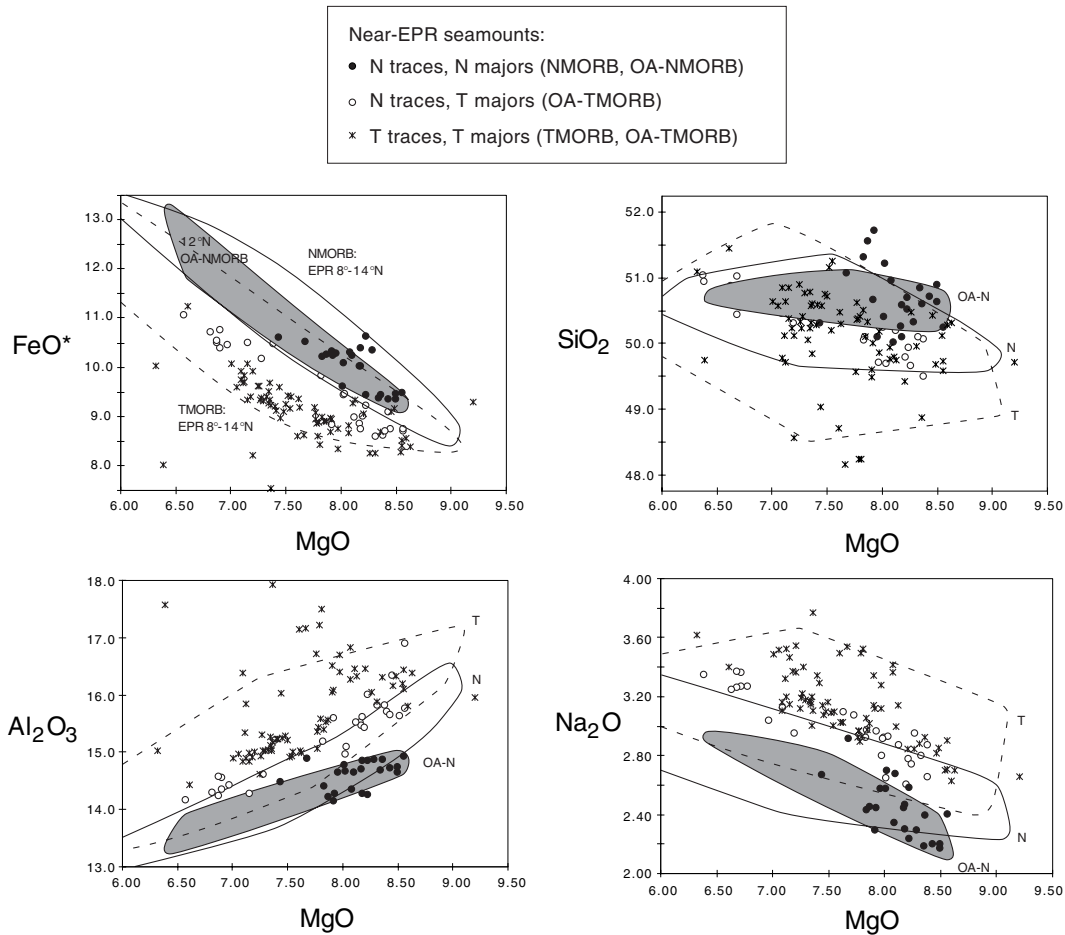


Figure 7. Glass compositions from near-EPR seamounts, compared with NMORB (solid lines) and TMORB (dashed lines) data fields from the EPR axis 8°–14°N. The shaded fields represent the 12°N OA-NMORB. Seamount samples with trace elements in the EPR NMORB field are divided into two groups. Solid circles are those that also have major elements in the NMORB or OA-NMORB field ($n = 21$). Open circles are those with major elements in the EPR TMORB field ($n = 29$); these samples are inferred to be OA-TMORB, generated from TMORB-source mantle. Crosses are seamount samples that have both trace and major elements in the TMORB field ($n = 72$), shown for comparison with the OA-TMORB. Seamount data sources as in Figure 6.

tween buoyant mantle upwelling and melt focusing under the EPR produces a different spectrum of compositions for off-axis volcanism. *Batiza et al.* [1989], *Niu and Batiza* [1991], and *Niu et al.* [1996] initially pro-

posed that near-EPR seamount major element compositions reflect a shallowing of the mantle solidus away from the ridge, which requires a component of buoyant upwelling beneath the EPR. However, *Niu and Batiza*



[1997, 1998] argue for seamount lavas giving a representative sampling of the melting regime. *Wilson* [1992] favored highly focused active upwelling beneath the EPR and described near-EPR seamount lavas as deep melts of fertile heterogeneities in the mantle that escape focusing to the ridge axis, mix with depleted melts from refractory mantle, and react with that refractory mantle, before erupting at off-axis seamounts.

[39] The characteristics of the OA-NMORB suggest another possibility. OA-NMORB have similar major element compositions to low-TiFe_{7.3} NMORB from the EPR but have systematically lower incompatible trace element concentrations and more depleted trace element patterns. This is consistent with the OA-NMORB being melts from the EPR melting regime that are incompletely pooled in the sense that they are missing the deep, low-degree melt fraction [*Reynolds*, 1995]. A similar explanation was proposed by *Allan et al.* [1989] and by *Niu and Batiza* [1991], to account for the unusually depleted trace element compositions of the Lamont Seamounts. These deep melts would have strong leverage on the incompatible trace element compositions of a pooled melt but would have little effect on more compatible trace elements or major elements. *Spiegelman's* [1996] calculations of two-dimensional (2-D) patterns of mantle flow and melt transport under ridges predict specific geochemical patterns in lavas, and for the case of passive mantle upwelling combined with melt focusing, the geochemical contrast between on-axis and off-axis lavas is remarkably similar to what we observe at the EPR. In his calculation, magmas erupted a short distance (several kilometers) off axis are systematically more depleted in trace elements but show no significant difference in major element compositions. This is because the deepest, least depleted melts are more

strongly focused to the ridge axis and are lost to these off-axis magmas. The close correspondence between *Spiegelman's* model and the geochemical data presented here points to dominantly 2-D mantle flow with melt focusing beneath the EPR, without a significant component of active upwelling. Quantitative comparison of this model with the 12°N data set is addressed more extensively by *Spiegelman and Reynolds* [1999].

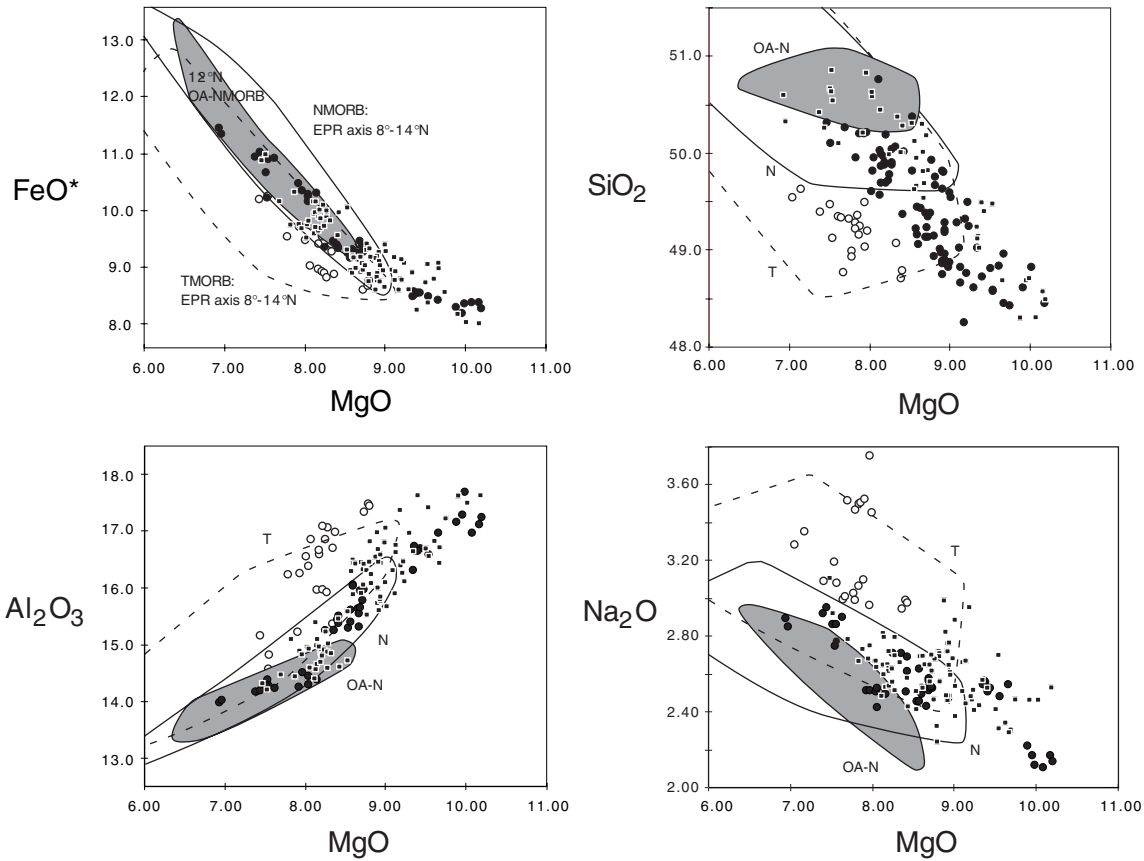
7. OA-TMORB Among the Enriched Basalts

[40] The discussion above has focused on the unusually depleted OA-NMORB, but it is well known that off-axis volcanism also produces enriched lavas on seamounts [e.g., *Batiza and Vanko*, 1984; *Niu and Batiza*, 1997, 1998]. Some of these enriched lavas may represent the same petrological phenomenon as OA-NMORB but from an enriched mantle source. By analogy with the OA-NMORB, an OA-TMORB should also be less enriched than expected from the mantle source composition. In the 12°N data set, VE7-A, VE24-D, VE29-B, and VE30 have transitional major and trace element compositions (Tables 1–3). However, comparison to the other TMORB suggests that they are offset from those compositions in the same direction as are the OA-NMORB in comparison with the axis NMORB, e.g., toward a combination of lower Fe_{7.3}, Ti_{7.3}, and Al_{7.3}, higher Si_{7.3} and Ca_{7.3} at constant Fe_{7.3}, and lower Na_{7.3} and Sr at constant TiFe_{7.3}. Thus these samples are possible OA-TMORB, equivalent to the OA-NMORB but from a moderately enriched mantle source that could have generated TMORB.

[41] It is difficult to devise a general OA discriminant for enriched samples. For depleted samples, reference can be made to the well-defined correlations between major and trace



Lamont Seamounts:
• small cones: N traces, N majors
• large seamounts: N traces, N majors
○ large seamounts: N traces, T majors (OA-TMORB)





element concentrations in the ridge axis lavas, but for enriched compositions such a reference frame is not well defined. The boundary between depleted and transitional MORB, however, is a useful reference.

[42] The NMORB-TMORB boundary has been defined in previous EPR studies in terms of various trace element ratios such as K_2O/TiO_2 , Ba/TiO_2 , La/Sm_N , Ce/Yb_N , and Nb/Zr . This boundary is the point at which increasing geochemical enrichment begins to dominate variations in trace element compositions (after correction for low-pressure fractionation). All of these trace element definitions are effectively identical in terms of whether an EPR sample is classified as NMORB or TMORB. This boundary also corresponds to a point where enrichment in trace elements begins to correlate with geochemical variations in the major elements; for example, increasing K_2O/TiO_2 begins to correlate with increasing $Na_{7.3}$ and $Al_{7.3}$ and decreasing $Fe_{7.3}$ [Langmuir *et al.*, 1992]. This is the case for EPR axis basalts.

[43] Among off-axis and seamount basalts the relationship between major and trace elements is more complex. As discussed in section 5, a large number of seamount samples with depleted (N-type) trace elements have transitional (T-type) major element compositions (Figures 7 and 8): 22 samples from the Lamont Seamounts [Zindler *et al.*, 1984; Fornari *et al.*, 1988; Allan *et al.*, 1989]; 28 samples from the near-ridge seamount samples of Batiza and

Vanko [1984], Batiza *et al.* [1989], and Allan *et al.* [1994]; and 9 samples of those published by Niu and Batiza [1997, 1998]. These represent 23, 22, and 16% of the samples with depleted trace element patterns in the respective data sets. There are similar compositions from off-axis dredges in the CHEPR data set: CH14.5 ($12^\circ 55'N$), CH15.2 ($12^\circ 51'N$), CH101.2 ($10^\circ 13'N$), and perhaps CH35.3 ($11^\circ 42'N$) and CH112.2 ($11^\circ 24'N$).

[44] One explanation for the characteristics of these samples is that they are OA-TMORB. In this scenario these samples reflect depletion of the incompatible elements from a mineralogically distinct portion of the mantle that gives rise to TMORB. The physical mechanism of loss of low-degree melts would be the same for OA-NMORB and OA-TMORB; the source involved would differ. Preservation of the major element characteristics of TMORB in the absence of the trace element enrichment implies a mineralogical control on the distinctive major element signature of TMORB that goes along with the trace element enrichment, as suggested previously [Prinzhofer *et al.*, 1989; Cousens, 1996; Hirschmann and Stolper, 1996].

8. Volcanological Implications of the Off-Axis Magma Type

[45] The recognition of the off-axis magma type allows a further consideration of the

Figure 8. Glass compositions from the Lamont Seamounts, compared with EPR data fields as in Figure 7. All Lamont Seamount samples reported in the literature have depleted trace element compositions. Samples from large Lamont Seamounts and from surrounding small cones resemble the $12^\circ N$ OA-NMORB. The major element compositions of other large Lamont Seamount glasses scatter toward more "enriched" compositions, and these are inferred to be OA-TMORB. Squares, samples from small cones around the base of Lamont Seamounts ($n = 45$); solid circles, depleted samples from large Lamont Seamounts (Sasha, MIB, MOK, NEW, DTD) ($n = 87$); open circles, samples from large Lamont Seamounts that have enriched major element compositions resembling TMORB ($n = 22$). Data are from Allan *et al.* [1989], adjusted as described in Figure 6.



Table 3. DCP Analyses of Major and Trace Elements^a

		SiO ₂	MgO	CaO	MnO	TiO ₂	Fe ₂ O ₃	Na ₂ O	K ₂ O	Al ₂ O ₃	P ₂ O ₅	Sum	Ba	Sr	Zr	Y	V	Zn	Sc	Cu	Ni	Cr	K ₂ O/TiO ₂
<i>OA-NMORB</i>																							
VE3-A	VE3-2	49.65	7.88	12.10	0.189	1.38	11.28	2.43	0.069	14.58	0.120	99.67	6.8	99	97	33.3	325	74	41.8	80	80	311	0.050
VE3-B	VE3-5	49.99	8.65	12.85	0.176	1.03	10.35	2.19	0.037	14.70	0.088	100.07	4.5	76	69	27.8	290	74	41.1	93	93	385	0.036
VE5-A	VE5-4	49.45	7.92	11.66	0.190	1.34	11.14	2.65	0.059	15.11	0.124	99.64	4.8	102	96	33.2	304	76	40.4	79	80	242	0.044
VE8-A	VE8-7	49.96	7.37	11.41	0.195	1.51	11.78	2.62	0.079	14.36	0.135	99.42	7.3	102	103	35.2	341	83	41.0	68	74	176	0.052
VE8-B	VE8-2	50.16	8.18	12.09	0.182	1.30	10.84	2.49	0.069	14.72	0.127	100.16	5.8	101	87	31.3	293	80	40.8	75	91	361	0.053
VE10	VE10-6	50.08	7.80	12.00	0.193	1.45	11.50	2.53	0.057	14.32	0.129	100.06	6.5	104	96	33.4	320	87	42.9	76	77	215	0.039
VE16	VE16-1	50.14	7.68	11.76	0.191	1.45	11.53	2.54	0.073	14.41	0.132	99.90	6.3	103	96	34.2	326	79	41.8	72	79	221	0.051
VE24-A	VE24-1	49.82	6.42	10.30	0.227	1.93	14.10	2.84	0.095	13.65	0.179	99.56	8.1	97	132	44.7	407	95	40.7	63	51	58	0.049
VE24-B	VE24-3	50.01	7.43	11.46	0.201	1.45	12.08	2.57	0.074	14.31	0.130	99.72	6.3	94	99	35.1	337	86	41.6	71	64	127	0.051
VE29-A	VE29-11	50.05	7.21	11.16	0.202	1.65	12.33	2.60	0.098	14.16	0.162	99.63	9.1	97	115	39.7	363	89	41.2	70	74	198	0.059
VE29-C	VE29-3	49.55	9.15	13.05	0.170	0.95	10.02	2.09	0.044	15.02	0.075	100.13	3.9	73	52	25.1	269	72	40.6	85	110	433	0.046
<i>"In Between" OA-NMORB and NMORB</i>																							
VE6	VE6-1	49.52	7.05	11.12	0.207	1.88	12.84	2.52	0.114	13.70	0.177	99.13	10.8	98	127	41.9	380	99	40.6	61	67	144	0.061
VE26	VE26-3	49.89	7.14	11.18	0.203	1.72	12.53	2.64	0.106	14.14	0.168	99.72	9.9	104	126	40.5	367	88	41.8	73	72	172	0.062
VE27-C	VE27-11	49.99	8.20	12.21	0.176	1.33	10.66	2.49	0.079	14.85	0.123	100.12	6.9	111	91	31.2	294	74	42.5	76	94	371	0.060
<i>OA-TMORB</i>																							
VE7-A	VE7-3	49.26	7.94	12.01	0.180	1.54	10.60	2.80	0.165	14.77	0.166	99.43	20.5	156	108	30.9	288	75	40.7	72	89	313	0.107
VE24-D	VE24-12	49.65	6.78	11.09	0.193	1.98	11.71	3.15	0.405	14.40	0.248	99.60	37.3	170	155	39.0	344	83	42.0	80	60	140	0.205
VE29-B	VE29-8	49.57	8.06	11.88	0.186	1.45	10.70	2.75	0.133	15.33	0.155	100.20	15.2	143	108	32.1	291	76	41.5	77	96	354	0.092
VE30	VE30-4	49.82	6.67	10.77	0.192	1.94	11.65	3.21	0.371	14.69	0.250	99.56	39.0	169	156	39.4	356	83	40.8	81	61	148	0.192
JDF-D2	standard	50.1	6.75	10.73	0.218	1.86	13.4	2.74	0.215	13.63	0.230	99.87	22	116	158	48	350	100	41.6	62	58	83	0.116
s.d., ppm		0.46	0.39	0.46	0.50	0.56	0.26	0.85	2.77	0.60	1.65		6	14	2	1.1	1.4	3	0.8	3	15	25	2.83

^aMajor and trace element compositions of bulk glasses from OA-type dredge samples in the 12°N study area. Handpicked glasses were analyzed by direct current plasma spectrometer (DCP) at Lamont-Doherty Earth Observatory. All samples within a given dredge that have a particular composition, within microprobe analytical precision, are assigned a single probe identification. Sample name is the individual sample analyzed by DCP. The Lamont standard JDF-D2 was used in calibrations of all DCP and microprobe analyses. Here, s.d., standard deviation.



organization and plumbing of volcanism around the EPR. On-axis eruptions occur in a zone of faults and fissures along the axis of the EPR that is 200–600 m wide in the 12°N region. This fissure zone is typically located within an axial summit trough [e.g., *Perfit and Chadwick*, 1998; *Fornari et al.*, 1998]. Off-axis eruptions are those that erupt through vents outside the axial fissure zone. Without knowledge of the field relations it is difficult to determine whether anomalously fresh lavas found off axis have truly erupted from off-axis vents, because large eruptions at the axis can also send lava flows up to several kilometers away [*Gente et al.*, 1986; *Barone and Ryan*, 1990; *Reynolds*, 1995]. Furthermore, the off-axis vents could erupt either lava transported laterally from the axial magma system or vertically from off-axis magma systems. Thus there is a zone where young lava flows emplaced off axis may come from the axial crustal plumbing system through vents on or off axis, or may come from off-axis magma systems that are independent of the axial plumbing.

8.1. Width of the Neovolcanic Zone: Evidence From 9°N

[46] A widely used definition of the neovolcanic zone of the EPR is the volcanically active, narrow fissure zone at the ridge axis, typically <250 m wide, in which volcanic and intrusive activity is concentrated [e.g., *Perfit and Chadwick*, 1998]. A somewhat expanded definition is the zone of active volcanism roughly centered on the axial fissure zone, though not necessarily confined to it [e.g., *Goldstein et al.*, 1994]. We use this latter definition, but with one modification. The zone of all active volcanism associated with the spreading center extends to the edge of the influence of the subridge melting regime and includes at minimum the

zone of near-ridge seamount initiation out to 10 km off axis [*Scheirer and Macdonald*, 1995; *Keeley et al.*, 1995]. We restrict the definition of the neovolcanic zone to the zone of active volcanism roughly centered around the EPR axis, through which lavas erupt from the axial magma system.

[47] Extensive on- and off-axis sampling and *Alvin* dives have been conducted in the region between 9°30'N and 9°52'N [*Perfit et al.*, 1994a, b]. On the basis of visual observations of seafloor terrain during *Alvin* dives, small-scale variability in lava compositions off axis, and an asymmetrical distribution of MgO and incompatible element enrichments in basalt compositions around the ridge axis at 9°30'–9°32'N, *Perfit et al.* [1994a, b] and *Fornari et al.* [1998] have concluded that a significant part of the seafloor outside the summit caldera has been covered by lavas erupted from off-axis vents. Anomalously young ages of some of the samples, as measured by U-series isotopic disequilibrium [*Goldstein et al.*, 1994], are the most convincing geochemical evidence of off-axis eruptions. *Perfit et al.* suggest that the petrological characteristics of the samples recovered off axis, particularly their heterogeneity, reflect a combination of (1) rapid changes in the composition of the axial melt lens combined with a wide neovolcanic eruption zone, and (2) additional off-axis eruptions from relatively small magma bodies, including TMORB and EMORB, that may be independent of the main melt lens that supplies lava to the axial summit caldera [*Perfit et al.*, 1994a]. On the basis of U-series ages of anomalously young off-axis basalts, *Goldstein et al.* [1994] conclude that most were erupted 0.5–2 km from the axis, with one sample (R49-1) erupting as far as 4 km off axis. Since they found evidence of active volcanism close to the outer edge of their study area, their ~2–4 km outer boundary of this



zone of active volcanism is a minimum estimate. They referred to all of this active off-axis volcanism as “neovolcanic.”

[48] The anomalously young 9°N samples include both NMORB and TMORB. We have examined the published NMORB data from 9°31'N [Perfit *et al.*, 1994a; Batiza and Niu, 1992] to see whether they correspond to the OA-NMORB magma type. The on-axis samples are all ordinary-looking NMORB, as is the single off-axis sample with a U-series date that matches the age predicted from the spreading rate. Of the five anomalously young off-axis samples, one is a TMORB, two are ordinary NMORB, and two are OA-NMORB (ARC38, R49-1). The observation that some are ordinary NMORB rather than OA-NMORB supports the suggestion of Perfit *et al.* [1994a] that some lavas emplaced off axis may come from the axial melt lens, while others do not. Identification of the OA-NMORB type helps us to determine which lavas come from which kind of magma system.

[49] Sample R49-1 was dredged 3.8 km east of the axis but is essentially zero age, according to both ²³⁰Th and ²³¹Pa secular disequilibrium. According to the criteria defined by 12°N samples, R49-1 is an OA-NMORB that probably did not erupt from the axial magma system and thus does not define the neovolcanic zone. Thus all of the anomalously young samples at 9°31'N with normal axis-type compositions were emplaced within ~2 km of the EPR axis. This may represent the limit of eruptions from the 9°N axial melt lens, i.e., the neovolcanic zone as we have defined it. The two OA-NMORB, erupted 1.3 and 3.8 km off axis, indicate the beginning of seamount-type eruptions rather than a continuation of ridge axis volcanism. In the 9°31'N region these two kinds of volcanism overlap in the zone from 1 to 2 km off axis.

8.2. Initiation and Areal Extent of Off-Axis Volcanism

[50] The OA-NMORB erupt as close as 1 km from the ridge axis in the 9°N and 12°N areas. Since these eruptions do not necessarily form volcanic constructions that are recognizable from bathymetry against the background of abyssal hill terrain, morphological studies to estimate the extent of off-axis volcanism lead to underestimates. For example, previous conclusions that seamount volcanism starts at ~5 km off axis [Scheirer and Macdonald, 1995; Alexander and Macdonald, 1996] or even 2 km [Keeley *et al.*, 1995], were limited by the resolution of multibeam bathymetric mapping systems to subcircular edifices at least 40 m high. It appears that eruptions from off-axis magma systems, and the initiation of seamount construction, actually begin as close as 1 km from the axial fissure zone.

[51] These off-axis magmas must pass through the crust close to the ridge axis. Seismic measurements of the full width of the axial melt sill in the 9°N region range from 500 to 1200 m (with one extreme value at 4100 m) [Kent *et al.*, 1993]. On the southern EPR, measurements of the sill width range from 300 to 1540 m [Kent *et al.*, 1994; Hooft *et al.*, 1997]. Seismic attenuation measurements at 9°30'N place a limit of 1–2 km on the full width of the magma chamber defined as a region containing more than a few percent melt [Wilcock *et al.*, 1995]. Even if the magma chamber is not centered on the ridge axis, it is possible that off-axis magmas may erupt as close as 1 km from the axis without being intercepted by the axial magma system. In fact, the correspondence between the seismic results and minimum off-axis distance of OA-type lavas suggests that the width of the axial magma body may be the factor that limits the proximity of OA-type eruptions to the ridge axis, because of that potential for interception.



[52] Previous estimates of the areal extent of off-axis volcanism around the northern EPR have also relied on identification of seamounts in bathymetric maps. Seamounts taller than 200 m form between 5 and 15 km and cover 6% of the seafloor [Scheirer and Macdonald, 1995]. Seamounts 40–200 m high form between 5 and 10 km and cover 7–11% of the seafloor [Alexander and Macdonald, 1996]. The sum of the two size ranges is 13–17%, but this is an overestimate because smaller seamounts that develop into larger ones over time [Fornari *et al.*, 1987; Keeley *et al.*, 1995; Alexander and Macdonald, 1996], as they move from 5 to 15 km off axis, would be counted twice. Thus the area covered by near-ridge seamounts >40 m high is probably closer to the maximum estimate for the smaller ones, ~11% of the seafloor.

[53] However, on the basis of the 12°N data, it appears that the areal extent of off-axis eruptions is significantly larger if flows and edifices <40 m high are included. In our study area, 39% of the dredges from >1 km off axis that contain depleted samples (55% with “in between” samples) and 33% of the depleted rock core samples from >1 km off axis (43% with “in between” samples) are OA-NMORB. Examination of the SeaMARC I sonar images and the seafloor photos suggests that this is higher than the proportion of the 12°N seafloor actually covered by off-axis eruptions. The combination of petrological and geological information suggests that off-axis eruptions in the 12°N region form a thin veneer over 10–40% of the seafloor, perhaps ~20%.

9. Conclusions

[54] Sampling of lavas off axis around the EPR, along with geological study of sampling locations, has brought to light a distinctive magma composition that can be used to identify off-

axis eruptions that do not come from the axial magma system. This OA-NMORB magma type, which is not found on the ridge axis (except at a ridge-transform intersection) but can occur as close as 1 km to the axis, is a widespread phenomenon near the northern EPR. It appears to represent the initial eruptions that in some cases subsequently lead to the formation of off-axis seamounts.

[55] The OA-NMORB compositions are characterized by unusual depletion in trace elements, with lower concentrations and ratios of incompatible trace elements than EPR lavas. Their major element compositions are similar to low-TiFe_{7.3} NMORB from the EPR axis, except that they are characterized by a combination of low Fe_{7.3} and Ti_{7.3} with low Na_{7.3}, Sr, and incompatible trace elements. A number of moderately enriched OA-TMORB, which differ from EPR TMORB in the same way that OA-NMORB differ from axial NMORB, are identified as well. The OA-NMORB compositions have strong affinities to depleted lavas from near-EPR seamounts. Moderately enriched seamount lavas show the same compositional tendencies; those with trace elements in the range of NMORB and major elements in the range of TMORB are interpreted as OA-TMORB.

[56] The geological evidence for off-axis eruption of the OA-NMORB in the 12°N region is compelling, but limited in extent. The observation that the petrological discriminant reveals no OA-NMORB within 1 km of the EPR axis 8°N–14°N (except one at a transform fault), yet several were recovered dredges farther off axis, is strong circumstantial support. The correspondence between the petrological systematics of OA-NMORB and the compositions and U-series dating of 9°N lavas [Batiza and Niu, 1992; Perfit *et al.*, 1994a; Goldstein *et al.*, 1994] provides direct geochemical evidence that identifies several OA-NMORB as off-axis



eruptions. The coherence of OA-NMORB and OA-TMORB is consistent with the overall physical model. The combination of these lines of evidence makes the case for OA-NMORB as an off-axis magma type.

[57] The areal extent of off-axis volcanism around the EPR is more extensive than previously realized. In the 12°N region it forms a thin veneer over 10–40% of the seafloor, probably ~20%. These off-axis flows are interspersed with large lava flows associated with the neovolcanic zone that travel out from the EPR axis [Reynolds, 1995] to thicken the off-axis volcanic layer of the ocean crust, as observed in seismic studies [e.g., Christeson *et al.*, 1996].

[58] We propose that the small off-axis eruptions of OA-NMORB and OA-TMORB should be viewed as the initiation of seamount-type off-axis volcanism. The zone of EPR axis volcanism, defined as eruptions from the axial magma system, overlaps the zone of seamount generation between 1 and 2 km from the ridge axis. The zones are not separated by a spatial gap, as previously implied.

[59] The distinctive depleted character of off-axis magmatism appears to be a general characteristic near the EPR and may be a natural consequence of melt focusing toward the ridge. Further upwelling of mantle that has lost low-degree melts will deliver the distinctive off-axis magma type to off-axis vents. In this case, off-axis lava compositions do not reflect the same range of chemical variation as magmas that erupt in the axial volcanic zone.

Appendix: Fractionation Correction

[60] Fractionation corrections in this paper are a slight departure from our earlier method [e.g., Reynolds *et al.*, 1992]. For the major element

oxides the form of the equation is $[C_{7.3} = C_i + (\text{MgO} - 7.3)b]$, where C_i is the measured concentration in the sample and $C_{7.3}$ is the concentration corrected to 7.3% MgO. We use linear slopes that match calculated liquid lines of descent for low-pressure olivine-plagioclase-clinopyroxene (ol-pl-cpx) fractionation in EPR compositions, using the computer program of Weaver and Langmuir [1990] as recalibrated by Langmuir *et al.* [1992]. The exception is Al_2O_3 . The Al_2O_3 trends in several subsets of the data are significantly flatter than the calculated LLD but are consistent with one another, e.g., among pairs of samples from individual dredges, samples from ~1 km east of the axis (same age?), and the samples identified as off-axis eruptions (discussed below). We use an Al_2O_3 slope defined by the data. The calculated SiO_2 slope varies significantly depending on the starting lava composition. However, the error introduced by using an average calculated SiO_2 slope, rather than the range of calculated slopes, is within the analytical precision of SiO_2 , so we use the average. For the minor elements TiO_2 , Na_2O , K_2O , and P_2O_5 and all trace elements, we use a fractionation correction of the form $[C_{7.3} = C_i(1 - F_{7.3})^{(1 - D)}]$, where $F_{7.3}$ is the amount of fractionation along an ol-pl-cpx cotectic needed to reach 7.3% MgO and D is the bulk distribution coefficient. The equation for $F_{7.3}$ has been derived from LLD calculations of F as a function of ΔMgO along an ol-pl-cpx cotectic, in EPR basalt compositions. The bulk distribution coefficients D match the subsets of the 12°N EPR data mentioned above. Equations for the fractionation corrections are given in the caption to Figure 4.

[61] These corrections are now internally consistent and match what is expected for simple, low-pressure fractionation of EPR basalt magmas. The main difference from linear corrections determined empirically from the overall slopes of the data is that the liquid lines of



descent (LLDs) of trace elements now curve as they should, and depend on initial concentration levels, and the new correction slopes for incompatible elements are less steep than the empirical ones. This implies that we are interpreting the apparent overenrichment trends of these elements as an en echelon series of trends resulting from “normal” fractionation of a range of parental magmas. This requires that the MgO correlate with the degree of enrichment of the parental magma. Justification for this approach comes from recent work on plagioclase-hosted melt inclusions by *Sours-Page et al.* [1999], who found that the K₂O (and, probably, P₂O₅) concentrations in the melt inclusions from individual depleted samples formed trends parallel to calculated LLDs, while the suite of depleted samples as a whole formed a steeper trend when plotted against Mg number. Furthermore, there was also a very good correlation between the average fractionation-corrected K₂O in melt inclusions from a sample and the K₂O in the host glass. These observations suggest that the melt inclusions represent components that mixed to form the parent to the host magma and that the apparent overenrichment trends of incompatible trace elements in the lavas reflect parental magma variations and melt aggregation processes, not fractionation alone. Because we are interested in the parental magma compositions, we run our fractionation corrections along calculated LLDs.

Acknowledgments

[62] The central role of Bill Ryan and Kim Kastens in the study of geological data from the 12°N region, a key starting point for this paper, is gratefully acknowledged. That geological study will be presented in depth in a separate publication. Detailed discussions with Marc Spiegelman about the 12°N data, fractionation corrections, sample classifications, and off-axis volcanism were greatly appreciated and contributed to the development of the paper. This paper has benefited from formal reviews

by Rodey Batiza, Roger Nielsen, and Brian Cousens and informal review by Dave Clague. We also thank Rodey Batiza for providing us with then-unpublished seamount data while this study was underway. This research was supported by the National Science Foundation and by a Postdoctoral Research Fellowship from the Monterey Bay Aquarium Research Institute. This is Lamont-Doherty Earth Observatory contribution number LDEO 6074.

References

- Alexander, R. T., and K. C. Macdonald, Small off-axis volcanoes on the East Pacific Rise, *Earth Planet. Sci. Lett.*, *139*, 387–394, 1996.
- Allan, J. F., R. Batiza, M. R. Perfit, D. J. Fornari, and R. O. Sack, Petrology of lavas from the Lamont Seamount chain and adjacent East Pacific Rise, 10°N, *J. Petrol.*, *30*, 1245–1298, 1989.
- Allan, J. F., R. Batiza, and R. O. Sack, Geochemical characteristics of Cocos Plate seamount lavas, *Contrib. Mineral. Petrol.*, *116*, 47–61, 1994.
- Babcock, J. M., A. J. Harding, G. M. Kent, and J. A. Orcutt, An examination of along-axis variation of magma chamber width and crustal structure on the East Pacific Rise between 13°30'N and 12°20'N, *J. Geophys. Res.*, *103*, 30,451–30,467, 1998.
- Barone, A. M., and W. B. F. Ryan, Single plume model for asynchronous formation of the Lamont Seamounts and adjacent East Pacific Rise terrains, *J. Geophys. Res.*, *95*, 10, 801–10, 827, 1990.
- Batiza, R., and Y. Niu, Petrology and magma chamber processes at the East Pacific Rise ~9°30'N, *J. Geophys. Res.*, *97*, 6779–6797, 1992.
- Batiza, R., and D. Vanko, Petrology of young Pacific seamounts, *J. Geophys. Res.*, *89*, 11,235–11,260, 1984.
- Batiza, R., T. L. Smith, and Y. Niu, Geological and petrological evolution of seamounts near the EPR based on submersible and camera study, *Mar. Geophys. Res.*, *11*, 169–236, 1989.
- Batiza, R., Y. Niu, and W. C. Zayac, Chemistry of seamounts near the East Pacific Rise: Implications for the geometry of subaxial mantle flow, *Geology*, *18*, 1122–1125, 1990.
- Christeson, G. L., G. M. Kent, G. M. Purdy, and R. S. Detrick, Extrusive thickness variability at the East Pacific Rise, 9°–10°N: Constraints from seismic techniques, *J. Geophys. Res.*, *101*, 2859–2873, 1996.
- Cousens, B. L., Depleted and enriched upper mantle sources for basaltic rocks from diverse tectonic environments in the northeast Pacific Ocean: The generation of oceanic alkaline vs. tholeiitic basalts, in *Earth Processes: Reading the Isotopic Code*, *Geophys. Monogr.*



- Ser.*, vol. 95, edited by A. Basu and S. Hart, pp. 207–231, AGU, Washington, D. C., 1996.
- Crane, K., Structural evolution of the East Pacific Rise axis from 13°10'N to 10°35'N: Interpretations from SeamarC I data, *Tectonophysics*, 136, 65–124, 1987.
- Fornari, D. J., R. Batiza, and J. F. Allan, Irregularly shaped seamounts near the East Pacific Rise: Implications for seamount origin and rise axis processes, in *Seamounts, Islands, and Atolls*, *Geophys. Monogr. Ser.*, vol. 43, edited by B. H. Keating et al., pp. 35–47, AGU, Washington, D. C., 1987.
- Fornari, D. J., M. R. Perfit, J. F. Allan, R. Batiza, R. Haymon, A. Barone, W. B. F. Ryan, T. Smith, T. Simkin, and M. A. Luckman, Geochemical and structural studies of the Lamont Seamounts: Seamounts as indicators of mantle processes, *Earth Planet. Sci. Lett.*, 89, 63–83, 1988.
- Fornari, D. J., R. M. Haymon, M. R. Perfit, T. K. P. Gregg, and M. H. Edwards, Axial summit trough of the East Pacific Rise 9°–10°N: Geological characteristics and evolution of the axial zone on fast spreading mid-ocean ridges, *J. Geophys. Res.*, 103, 9827–9855, 1998.
- Gente, P., J. M. Auzende, V. Renard, Y. Fouquet, and D. Bideau, Detailed geological mapping by submersible of the East Pacific Rise axial graben near 13°N, *Earth Planet. Sci. Lett.*, 78, 224–236, 1986.
- Goldstein, S. J., M. R. Perfit, R. Batiza, D. J. Fornari, and M. T. Murrell, Off-axis volcanism at the East Pacific Rise detected by uranium-series dating of basalts, *Nature*, 367, 157–159, 1994.
- Harding, A. J., G. M. Kent, and J. A. Orcutt, A multi-channel seismic investigation of upper crustal structure at 9°N on the East Pacific Rise: Implications for crustal accretion, *J. Geophys. Res.*, 98, 13,925–13,944, 1993.
- Hirschmann, M. M., and E. M. Stolper, A possible role for garnet pyroxenite in the origin of the “garnet signature” in MORB, *Contrib. Mineral. Petrol.*, 124, 185–208, 1996.
- Hooft, E. E. E., H. Schouten, and R. S. Detrick, Constraining crustal emplacement processes from the variation in seismic layer 2A thickness at the East Pacific Rise, *Earth Planet. Sci. Lett.*, 142, 289–309, 1996.
- Hooft, E. E. E., R. S. Detrick, and G. M. Kent, Seismic structure and indicators of magma budget along the southern East Pacific Rise, *J. Geophys. Res.*, 102, 27,319–27,340, 1997.
- Kappus, M. E., A. J. Harding, and J. A. Orcutt, A baseline for upper crustal velocity variations along the East Pacific Rise at 13°N, *J. Geophys. Res.*, 100, 6143–6161, 1995.
- Keeley, C. D., A. Macario, W. B. F. Ryan, and W. F. Haxby, Simulating seamount populations for the southern East Pacific Rise and the Pacific/Antarctic Ridge, *Eos Trans. AGU*, 76(17), Spring Meet. Suppl., S273, 1995.
- Kent, G. M., A. J. Harding, and J. A. Orcutt, Distribution of magma beneath the East Pacific Rise between the Clipperton Transform and the 9°17'N Deval from forward modeling of common depth point data, *J. Geophys. Res.*, 98, 13,945–13,969, 1993.
- Kent, G. M., A. J. Harding, J. A. Orcutt, R. S. Detrick, J. C. Mutter, and P. Buhl, Uniform accretion of oceanic crust south of the Garrett Transform at 14°15'S on the East Pacific Rise, *J. Geophys. Res.*, 99, 9097–9116, 1994.
- Langmuir, C. H., *Petrology Data Base*, vol. 2 and 3, *East Pacific Rise Data Synthesis Final Report*, edited by S. Tighe, Joint Oceanogr. Inst., Washington, D. C., 1988.
- Langmuir, C. H., J. F. Bender, and R. Batiza, Petrologic and tectonic segmentation of the East Pacific Rise, 5°30'N–14°30'N, *Nature*, 332, 422–429, 1986.
- Langmuir, C. H., E. M. Klein, and T. Plank, Petrological systematics of mid-ocean ridge basalts: Constraints on melt generation beneath ocean ridges, in *Mantle Flow and Melt Generation at Mid-Ocean Ridges*, *Geophys. Monogr. Ser.*, vol. 71, edited by J. Phipps Morgan, D. K. Blackman, and J. M. Sinton, pp. 183–280, AGU, Washington, D. C., 1992.
- Macdonald, K. C., S. P. Miller, B. P. Luyendyk, T. M. Atwater, and L. Shure, Investigation of a Vine-Matthews magnetic lineation from a submersible: The source and character of marine magnetic anomalies, *J. Geophys. Res.*, 88, 3403–3418, 1983.
- Macdonald, K. C., P. J. Fox, R. T. Alexander, R. Pockalny, and P. Gente, Volcanic growth faults and the origin of Pacific abyssal hills, *Nature*, 380, 125–129, 1996.
- Monti, S., P. Gente, and J.-P. Maze, Carte bathymétrique de la dorsale Est-Pacifique de 10° Nord à 14°30' Nord, Inst. Fr. de Rech. pour l'Exploit. de la Mer, Brest, France, 1987.
- Niu, Y., and R. Batiza, An empirical method for calculating melt compositions produced beneath mid-ocean ridges: Application for axis and off-axis (seamounts) melting, *J. Geophys. Res.*, 96, 21,753–21,777, 1991.
- Niu, Y., and R. Batiza, Trace element evidence from seamounts for recycled oceanic crust in the eastern Pacific mantle, *Earth Planet. Sci. Lett.*, 148, 471–483, 1997.
- Niu, Y., and R. Batiza, Erratum to “Trace element evidence from seamounts for recycled oceanic crust in the eastern Pacific mantle,” *Earth Planet. Sci. Lett.*, 155, 147, 1998.
- Niu, Y., D. G. Wagoner, J. M. Sinton, and J. J. Mahoney, Mantle source heterogeneity and melting processes be-



- neath seafloor spreading centers: The East Pacific Rise, 18°–19°S, *J. Geophys. Res.*, *101*, 27,711–27,733, 1996.
- Perfit, M. R., and W. W. Chadwick Jr., Magmatism at mid-ocean ridges: Constraints from volcanological and geochemical investigations, in *Faulting and Magmatism at Mid-Ocean Ridges*, *Geophys. Monogr. Ser.*, vol. 106, edited by R. Buck et al., pp. 59–115, AGU, Washington, D. C., 1998.
- Perfit, M. R., D. J. Fornari, M. C. Smith, J. F. Bender, C. H. Langmuir, and R. M. Haymon, Small-scale spatial and temporal variations in mid-ocean ridge crest magmatic processes, *Geology*, *22*, 375–379, 1994a.
- Perfit, M. R., M. C. Smith, D. J. Fornari, M. H. Edwards, W. I. Ridley, S. J. Goldstein, J. F. Bender, and R. M. Haymon, Detailed petrological and geochemical studies of on- and off-axis lavas from the East Pacific Rise: 9°30'N–10°N, *Eos Trans. AGU*, *75*(44), Fall Meet. Suppl., 601, 1994b.
- Prinzhofer, A., E. Lewin, and C. J. Allegre, Stochastic melting of the marble cake mantle: Evidence from local study of the East Pacific Rise at 12°50'N, *Earth Planet. Sci. Lett.*, *92*, 189–206, 1989.
- Reynolds, J. R., Segment-scale systematics of mid-ocean ridge magmatism and geochemistry, Ph.D. dissertation, Columbia Univ., New York, 1995.
- Reynolds, J. R., and C. H. Langmuir, Petrological systematics of the Mid-Atlantic Ridge south of Kane: Implications for ocean crust formation, *J. Geophys. Res.*, *102*, 14,915–14,946, 1997.
- Reynolds, J. R., C. H. Langmuir, J. F. Bender, K. A. Kastens, and W. B. F. Ryan, Spatial and temporal variability in the geochemistry of basalts from the East Pacific Rise, *Nature*, *359*, 493–499, 1992.
- Scheirer, D. S., and K. C. Macdonald, Near-axis seamounts on the flanks of the East Pacific Rise, 8°N to 17°N, *J. Geophys. Res.*, *100*, 2239–2259, 1995.
- Sempere, J.-C., K. C. Macdonald, S. P. Miller, and L. Shure, Detailed study of the Brunhes/Matuyama reversal boundary on the East Pacific Rise at 19°30'S: Implications for crustal emplacement processes at an ultra fast spreading center, *Mar. Geophys. Res.*, *9*, 1–23, 1987.
- Sinton, J. M., S. M. Smaglik, J. J. Mahoney, and K. C. Macdonald, Magmatic processes at superfast spreading mid-ocean ridges: Glass compositional variations along the East Pacific Rise 13°–23°S, *J. Geophys. Res.*, *96*, 6133–6155, 1991.
- Sours-Page, R., K. T. M. Johnson, R. L. Nielsen, and J. L. Karsten, Local and regional variation of MORB parent magmas: Evidence from melt inclusions from the Endeavour Segment of the Juan de Fuca Ridge, *Contrib. Mineral. Petrol.*, *134*, 342–363, 1999.
- Spiegelman, M., Geochemical consequences of melt transport in 2-D: The sensitivity of trace elements to mantle dynamics, *Earth Planet. Sci. Lett.*, *139*, 115–132, 1996.
- Spiegelman, M., and J. R. Reynolds, Combined dynamic and geochemical evidence for convergent melt flow beneath the East Pacific Rise, *Nature*, *402*, 282–285, 1999.
- Weaver, J. S., and C. H. Langmuir, Calculation of phase equilibrium in mineral-melt systems, *Comput. Geosci.*, *16*, 1–19, 1990.
- Wilcock, W. S. D., S. C. Solomon, G. M. Purdy, and D. R. Toomey, Seismic attenuation structure of the East Pacific Rise near 9°30'N, *J. Geophys. Res.*, *100*, 24,147–24,165, 1995.
- Wilson, D. S., Focused mantle upwelling beneath mid-ocean ridges: Evidence from seamount formation and isostatic compensation of topography, *Earth Planet. Sci. Lett.*, *113*, 41–55, 1992.
- Zindler, A., H. Staudigel, and R. Batiza, Isotope and trace element geochemistry of young Pacific seamounts: Implications for the scale of upper mantle heterogeneity, *Earth Planet. Sci. Lett.*, *70*, 175–195, 1984.